Copy 6
RM L56E30a

NACA

RESEARCH MEMORANDUM

WIND-TUNNEL INVESTIGATION OF THE EFFECTS OF WING THICKNESS ON THE STATIC LONGITUDINAL AND LATERAL STABILITY OF UNSWEPT WINGS OF ASPECT RATIO 3 AT HIGH SUBSONIC SPEEDS

By William C. Hayes, Jr., and Edward C. Polhamus

Langley Aeronautical Laboratory
Langley Field, Va.

NATIONAL ADVISORY COMMITTEE FOR AERONAUTICS

WASHINGTON

August 23, 1956

NATIONAL ADVISORY COMMITTEE FOR AERONAUTICS

RESEARCH MEMORANDUM

WIND-TUNNEL INVESTIGATION OF THE EFFECTS OF WING THICKNESS ON THE STATIC LONGITUDINAL AND LATERAL STABILITY OF UNSWEPT WINGS OF ASPECT RATIO 3 AT HIGH SUBSONIC SPEEDS

By William C. Hayes, Jr., and Edward C. Polhamus

SUMMARY

An investigation was made to determine the effects of wing-thickness on the static longitudinal and lateral stability of a wing-fuselage combination at high subsonic speeds. The wings had an aspect ratio of 3, a taper ratio of 0.5, zero sweep of the half-chord line, and NACA 65A002, NACA 65A004, and NACA 65A006 airfoil sections parallel to the plane of symmetry. The variations of side force, yawing moment, and rolling moment with angle of sideslip were obtained as a continuous trace through the angle-of-sideslip range in order to detect any nonlinearities.

Below a Mach number of 0.90, wing thickness had little effect on the lift-curve slope; however, above a Mach number of 0.90 a considerable increase was obtained for the 2-percent-thick wing. An increase in maximum lift with decrease in wing thickness was noted throughout the Mach number range. A rearward movement of the aerodynamic-center location occurred at a lower Mach number than that predicted by theory. A decrease in drag due to lift with increase in wing thickness was noted through the Mach number range to 0.92, whereas at a Mach number of 0.95 the reverse was true.

The values of the rate of change of the effective dihedral parameter with lift coefficient were in fair agreement with theory except for a moderate increase with Mach number which was not predicted and which was greatest for the 6-percent-thick wing. Although wing thickness had little effect on directional stability, all three wing-fuselage combinations provided a desirable reduction in the wing-fuselage directional instability at the higher angles of attack.

[redacted]

INTRODUCTION

An extensive research program is being conducted in the Langley high-speed 7- by 10-foot tunnel to determine the effects of wing geometry on the static stability characteristics of wing-body combinations at high subsonic speeds. This program has included a systematic investigation of the effect of sweepback (ref. 1), aspect ratio (ref. 2), taper ratio (ref. 3), and geometric dihedral (ref. 4) on the longitudinal and lateral stability characteristics for Mach numbers up to about 0.95. In addition, the static stability of two delta plan-form wings has been investigated (refs. 5 and 6). A summary of the rolling moment due to sideslip characteristics for all these investigations has been published in reference 7.

Although the program is fairly complete with respect to plan-form characteristics, the effects of wing thickness have not been studied. In addition, the angle-of-attack range was rather limited - especially at the higher Mach numbers - and since (except for some limited data at low angles of attack) the lateral data were obtained at fixed sideslip angles ($\beta = \pm 4^{\circ}$), no indication of possible nonlinearities in directional stability in the very low sideslip range was obtained. Therefore, the purpose of the present investigation was to determine the effect of wing thickness on the static stability characteristics through a large angle-of-attack range for Mach numbers up to 0.95. Testing through a large angle-of-attack range was made possible by use of considerably smaller models than those used in the previous investigations; thereby, the tunnel power and choking limitations were alleviated. Also, in order to study possible nonlinearities in the low sideslip range, the models were tested on a variable-yaw sting which was designed to allow continuous records of the forces and moments to be obtained through the sideslip range.

Three wings having an aspect ratio of 3, a taper ratio of 0.5, zero sweep of the half-chord line, and NACA 65A002, NACA 65A004, and NACA 65A006 airfoil sections parallel to the plane of symmetry were tested.

COEFFICIENTS AND SYMBOLS

In figure 1 are shown the axis system and the positive directions of forces, moments, and angles used in presenting the data. With the exception of lift and drag, the data are presented about the body axes of the model. The center of moments is located at 25 percent of the mean aerodynamic chord of the wing.

C_L	lift coefficient, $\frac{\text{Lift}}{qS}$
C_D	drag coefficient, $\frac{\text{Drag}}{qS}$
ΔC_D	total drag coefficient minus drag coefficient at zero lift
C_m	pitching-moment coefficient, $\frac{\text{Pitching moment}}{qS\bar{c}}$
C_l	rolling-moment coefficient, $\frac{\text{Rolling moment}}{qSb}$
C_n	yawing-moment coefficient, $\frac{\text{Yawing moment}}{qSb}$
C_Y	lateral-force coefficient, $\frac{\text{Lateral force}}{qS}$
q	dynamic pressure, $\frac{\rho V_o^2}{2}$, lb/sq ft
ρ	mass density of air, slugs/cu ft
V_o	free-stream velocity, ft/sec
M	Mach number
S	wing area, sq ft
b	wing span, ft
$\bar{c}$	wing mean aerodynamic chord, $\frac{2}{S}\int_0^{b/2} c^2 dy$, ft
c	wing chord at any spanwise station, ft
t	maximum wing thickness at any spanwise station, ft
α	angle of attack, deg
β	angle of sideslip, deg
$\Lambda_{c/2}$	angle of sweepback of half-chord line, deg
R	Reynolds number

[redacted]

A wing aspect ratio, b^2/S

λ wing taper ratio, $\frac{\text{Tip chord}}{\text{Root chord}}$

X_{ac} distance to aerodynamic center measured from leading edge of wing mean aerodynamic chord

$C_{L_\alpha} = \frac{\partial C_L}{\partial \alpha}$

C_{Y_β} lateral-force coefficient due to sideslip, $\frac{\partial C_Y}{\partial \beta}$, per deg

C_{n_β} yawing-moment coefficient due to sideslip, $\frac{\partial C_n}{\partial \beta}$, per deg

C_{l_β} rolling-moment coefficient due to sideslip, $\frac{\partial C_l}{\partial \beta}$, per deg

$C_{l_{\beta C_L}}$ rate of change of C_{l_β} with lift coefficient, $\partial C_{l_\beta} / \partial C_L$

MODEL AND APPARATUS

Details of the complete model are presented in figure 2. The fuselage consisted of a cylindrical aluminum center section fitted with plastic nose and tail sections. With this fuselage were tested three stainless-steel wings having an aspect ratio of 3, a taper ratio of 0.5, zero sweep at the half chord, and NACA 65A002, NACA 65A004, and NACA 65A006 airfoil sections parallel to the plane of symmetry.

Schematic diagrams and photographs which illustrate the mechanical system used to obtain the continuous yaw records are presented in figure 3. With this system an angle-of-sideslip range of approximately -5° to 5° and an angle-of-attack range of -3° to 23° can be obtained by remote operation. The prime motivation of the system is a 1/4-horsepower electric motor which drives the piston within the master cylinder. The amount and direction of the movement of this piston is automatically controlled by a system of limit switches and clutches and is duplicated by the piston within the slave cylinder. Longitudinal movement transmitted from the slave cylinder to the sliding block is translated to lateral motion by means of a diagonal slot in the sliding block and a pivoted follower arm. The rate of change in sideslip angle β is approximately 1 degree per second which is believed to be slow enough to eliminate any appreciable effects of transient phenomena. Forces and moments are measured with a six-component strain-gage balance mounted within the model.

TESTS AND CORRECTIONS

Tests were made in the Langley high-speed 7- by 10-foot tunnel for a Mach number range from 0.60 to 0.95 corresponding to a Reynolds number range of 1.15×10^6 to 1.30×10^6 based on the wing mean-aerodynamic-chord length (0.299 foot). An angle-of-attack range of -3° to 23° was obtained at the lower Mach numbers. At the higher Mach numbers the angle-of-attack range was limited (0° to approximately 13° at $M = 0.95$) to avoid exceeding the design-load limits of the balance. An angle-of-sideslip range of approximately -5° to 5° was obtained at all test angles of attack. Jet-boundary corrections determined by the method of reference 8 and blocking corrections determined by the method of reference 9 were found to be negligible and therefore were not applied to the data. The angle of attack and angle of sideslip have been corrected for deflection of the sting support system and balance under load.

RESULTS AND DISCUSSION

Longitudinal Stability Characteristics

The basic lift, drag, and pitching-moment characteristics of the fuselage alone and the wing-fuselage combinations are presented in figures 4 to 8. The unrealistic drag coefficients indicated for the fuselage alone at low angles of attack are due to the fact that the drag on the fuselage alone was of the order of the accuracy of the balance which was designed to measure the large forces encountered by the wing-fuselage combination at high angles of attack. The upper part of figure 9 presents, as a function of Mach number, a comparison of the experimental lift-curve slopes for the three different wing thicknesses with estimates based on thin-airfoil theory. The variation of the theoretical lift-curve slope with Mach number was calculated by the method presented in appendix A of reference 7 using the method of reference 10 to account for the wing-fuselage interference. It will be noted that below a Mach number of about 0.90 there is relatively little effect of wing thickness and that the theory is in fair agreement with experimental values; however, above a Mach number of 0.90 the 2-percent-thick wing exhibited a considerably more rapid increase in lift-curve slope with Mach number than do the 4-percent- and 6-percent-thick wings. This is apparently due to the ability of the thinner wing to maintain (at an angle of attack) supersonic flow over a larger portion of the chord. (See refs. 11 and 12.)

The maximum lift values presented in the lower part of figure 9 represent the first peak and neglect the recovery of slope at the higher

[redacted]

angles of attack. The results indicate a rather large increase in maximum lift with decreasing wing thickness throughout the Mach number range investigated. It will be noted, however, that the variation with Mach number for the 2-percent-thick wing is somewhat different from that for the 4-percent- and 6-percent-thick wings, with a decrease occurring between 0.6 and 0.8. All three wings exhibit a rather rapid increase in maximum lift at the higher Mach numbers.

Figure 10 presents the variation of the aerodynamic-center location (aft of leading edge of mean aerodynamic chord) with Mach number for the three wings investigated. Also shown are the theoretical thin-airfoil estimates which were determined by the method of reference 10. (The method of reference 10 was modified slightly with regard to the subsonic wing alone center of pressure presented in figure 17 of reference 10 since the values differ considerably from those determined by the lifting-surface theory. Values from references 13 and 14 were used to replace the $\lambda = 1$ curve and were used as a guide to fair the curves for the other taper ratios into the slender-body values at $\beta A = 0$.) The experimental results indicate general agreement with theory in that the forward movement of the aerodynamic center associated with increasing induced camber is followed at the high Mach numbers by a rapid rearward movement associated with the establishment of chordwise loading of the supersonic type. It will be noted, however, that the experimental results for all three thickness ratios indicate a considerably more rapid forward movement and an earlier rearward movement than indicated by the theory. Both of these deviations are probably associated with the fact that the thickness- and lift-induced perturbation velocities cause an early establishment of local supersonic velocities on the wings which is neglected in the theory. The lack of progression toward the theory as the wing thickness is reduced is probably due to the fact that a reduction in thickness is accompanied by an increase in the effectiveness of lift coefficient in reducing the critical Mach number. This effect can, even at the low lift-coefficient range over which the aerodynamic-center locations were determined, cancel the favorable thickness effect which exists at zero lift. (See ref. 15.) The more rearward location of the aerodynamic center of the 2-percent- and 4-percent-thick wings relative to that for the 6-percent-thick wing may be associated with leading-edge separation which occurs on thin airfoils.

Figure 11 presents the variation of the drag-due-to-lift parameter with Mach number for each of the experimental wings compared in each case with the theoretical values for full leading-edge suction $1/\pi A$ and zero leading-edge suction $1/C_{L_\alpha}$ (see ref. 16), where C_{L_α} was determined from data of the present investigation. It will be noted that at Mach numbers up to approximately 0.92 the drag due to lift increased with decrease in wing thickness probably because of loss of leading-edge suction associated with the decrease in leading-edge radius. At the highest test Mach number the drag due to lift decreased with decrease in wing thickness because at this Mach number the resultant force is normal to the wing chord and, therefore, the thin wing with a higher lift-curve

slope has less drag due to lift. It is noted that in the case of the 2-percent-thick wing, the experimental values of drag due to lift are higher than the theoretical values which assume zero leading-edge suction. This is so probably because of the increase in profile drag associated with the forward movement of the transition with increase in lift coefficient. (See ref. 17.)

Lateral Stability Characteristics

The basic lateral-force, yawing-moment, and rolling-moment characteristics of the fuselage alone and the wing-fuselage combinations are presented in figures 12 to 15. As mentioned previously, the lateral-stability data were determined from continuous records of the force and moment variation with sideslip angle. The static-lateral-stability derivatives C_{Y_β}, C_{n_β}, and C_{l_β} were computed at each angle of attack by taking the algebraic difference between the values of the particular component at each of the limiting angles of sideslip ($\beta \approx \pm 5^\circ$). These values were then divided by the algebraic difference between the angles of sideslip. This is illustrated in sketch (a) for a linear variation of rolling moment with angle of sideslip and for which the value of C_{l_β} remained constant throughout the angle-of-sideslip range:

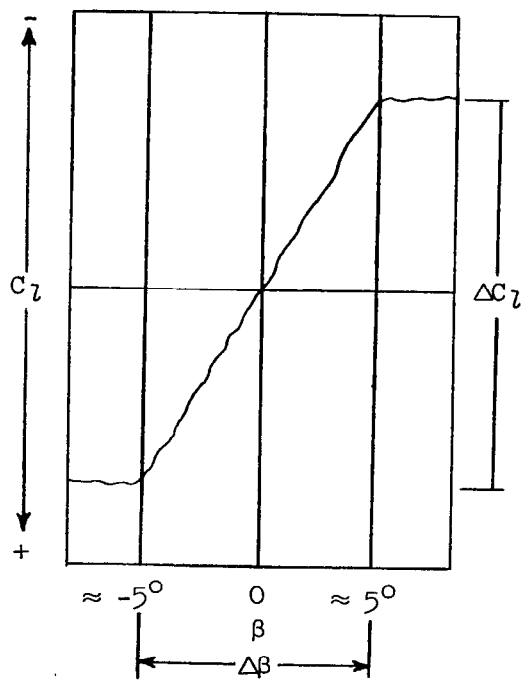

$$C_{l_\beta} = \frac{\Delta C_l}{\Delta \beta}$$

Sketch (a)

[redacted]

In some cases, however, the variations of side force, yawing moment, and rolling moment were nonlinear with angle of sideslip. Sketch (b) shows two sample traces of nonlinear variations of rolling moment with angle of sideslip. It should be noted that the same method was used to determine the derivatives as was employed in the cases of linear variation.

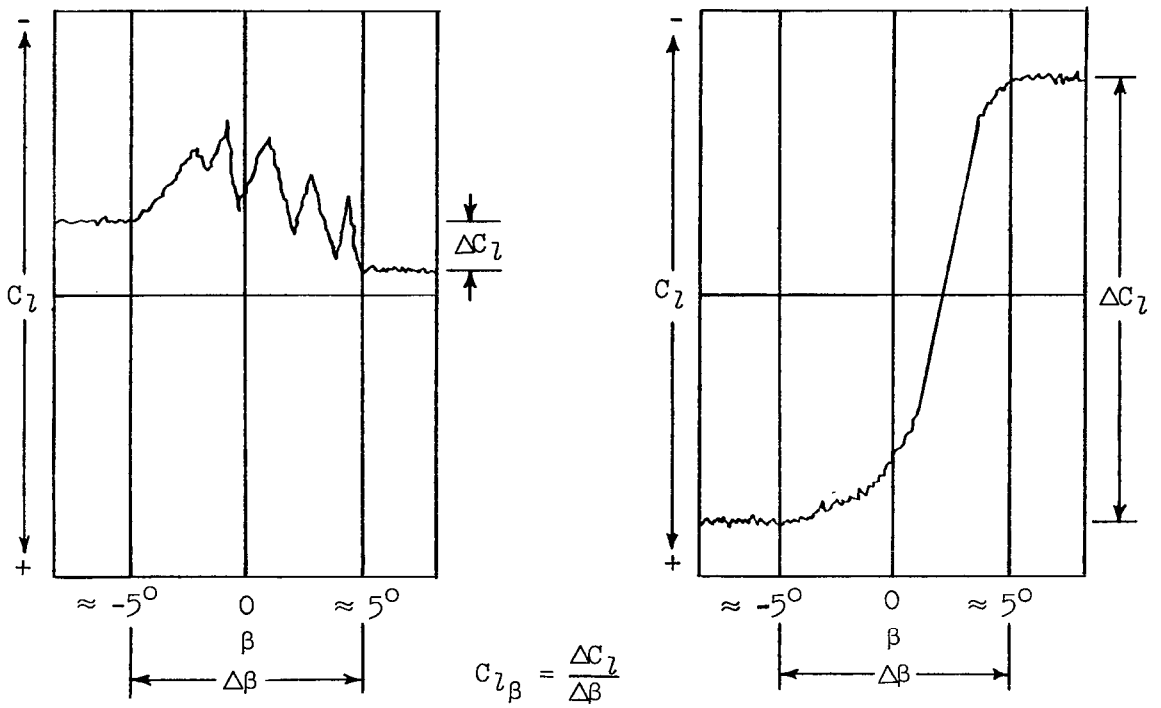

Sketch (b)

In order to differentiate between the derivatives obtained from linear or nonlinear variations with β, different types of symbols are used in figures 13 to 15. In these figures, open symbols are used to denote the angles of attack at which the variation of force or moment with angle of sideslip was considered linear (sketch (a)), whereas the solid symbols denote those angles of attack at which the variation was considered nonlinear (sketch (b)).

Inasmuch as the effect of wing thickness appears to be greatest for the effective dihedral parameter C_{l_β} and since the directional stability and side-force characteristics (C_{n_β} and C_{Y_β}, respectively) will be

[redacted]

affected to a large extent by the particular tail assembly used, the present discussion is mainly concerned with the effective dihedral parameter. In view of the fact that C_{l_β} is more closely associated with lift coefficient than angle of attack, a comparison of the variation of C_{l_β} with C_L for the different wing thicknesses is presented in figure 16 for the various Mach numbers investigated. With the exception of the highest Mach number the results indicate the effective dihedral parameter C_{l_β} to be a fairly linear function of lift coefficient below a lift coefficient of about 0.40. It can also be noted that in this range the effect of wing thickness and Mach number is relatively small. This is more clearly indicated in figure 17 where the slope $\left(C_{l_{\beta_{C_L}}}\right)$ of the curve of C_{l_β} plotted against C_L is presented as a function of Mach number for the three wing thicknesses. Also shown is an estimate by the method presented in reference 7. The experimental values are in fairly good agreement with the estimated values at low Mach numbers; however, the experimental results indicate a moderate increase with Mach number which is not predicted by the method of reference 7. Although there appears to be essentially no effect of wing thickness on $C_{l_{\beta_{C_L}}}$ between the 2-percent-thick and 4-percent-thick wings, the values for the 6-percent-thick wing are slightly larger throughout the Mach number range. It can be noted that at the higher Mach numbers where supersonic flow is fairly well established on the wings there is a decrease in $C_{l_{\beta_{C_L}}}$ as indicated in reference 7 for supersonic speeds.

Regarding the effective dihedral characteristics at high lift coefficients the results (fig. 16) indicate rather large effects of wing thickness, Mach number, and lift coefficient. The curves at the higher lift coefficients are characterized by a rapid increase in C_{l_β} with increasing lift coefficient. Wing thickness had a pronounced effect, with the increase occurring at higher lift coefficients as the thickness decreased. As the Mach number increased beyond 0.90, the effect of lift coefficient decreased, and at a Mach number of 0.95 little effect of lift coefficient or wing thickness occurred.

As mentioned previously, the variation of rolling-moment coefficient C_l with sideslip angle β was considerably nonlinear in some cases which are represented by solid symbols in the basic data. (See fig. 15.) This is illustrated in more detail in figure 18 where the characteristics of the 6-percent- and 2-percent-thick wings are compared at a Mach number of 0.85. For orientation with regard to lift coefficient, the upper part of the lift curve is also presented. Also shown are the continuous traces of rolling-moment coefficient as a function of sideslip angle from which the values of C_{l_β} were determined. From these traces it can be noted

that in the angle-of-attack range where there are large reductions in C_{l_β} associated with the thin wing, the variation with sideslip angle is very nonlinear and the derivative appears to be of little value. A more complete set of traces for all three wing thicknesses at this same Mach number is presented in figure 19.

Figure 20 presents the combinations of lift coefficient and Mach number for which nonlinear variations of rolling-moment coefficient with sideslip angle exist.

In connection with the directional-stability parameter C_{n_β}, it can be noted (fig. 14) that in addition to the fact that nonlinear variations with sideslip exist, the wing-fuselage instability generally decreases considerably at the higher angles of attack. This trend, which is desirable in view of the usual loss of vertical-tail contribution at high angles of attack, is opposite that obtained for sweptback wings and appears to be associated with a favorable wing interference on the fuselage afterbody. (See ref. 18.)

CONCLUSIONS

The results of a wind-tunnel investigation to determine the effects of wing thickness on static longitudinal and lateral stability characteristics of unswept wings of aspect ratio 3 at high subsonic speeds indicate the following conclusions:

1. Below a Mach number of 0.90 the lift-curve slope is little affected by wing thickness and shows fairly good agreement with theory. Above a Mach number of 0.90 the lift-curve slope for the 2-percent-thick wing exhibits a more rapid rise with increase in Mach number than do the thicker wings. Throughout the Mach number range the maximum lift decreases with an increase in wing thickness.

2. The aerodynamic centers of the 2-percent- and 4-percent-thick wings are somewhat rearward of that of the 6-percent-thick wing at subcritical speeds. All three wings exhibit the trends with Mach number indicated by theory but these trends occur at considerably lower Mach numbers than theory indicates.

3. The drag due to lift increases with decrease in wing thickness through the Mach number range from 0.60 to approximately 0.92. However, at a Mach number of approximately 0.95 the drag due to lift decreases with a decrease in wing thickness.

4. The values of the rate of change of the effective dihedral parameter with lift coefficient are in fair agreement with theory except for

a moderate increase with Mach number which was not predicted. The 6-percent-thick wing has a value which is slightly higher than those for the thinner wings.

5. Wing thickness has relatively little effect on the directional stability; all three wing-fuselage combinations provide a desirable reduction in the wing-fuselage instability at the higher angles of attack.

Langley Aeronautical Laboratory,
National Advisory Committee for Aeronautics,
Langley Field, Va., May 14, 1956.

REFERENCES

1. Kuhn, Richard E., and Fournier, Paul G.: Wind-Tunnel Investigation of the Static Lateral Stability Characteristics of Wing-Fuselage Combinations at High Subsonic Speeds - Sweep Series. NACA RM L52G11a, 1952.

2. Fournier, Paul G., and Byrnes, Andrew L., Jr.: Wind-Tunnel Investigation of the Static Lateral Stability Characteristics of Wing-Fuselage Combinations at High Subsonic Speeds. Aspect-Ratio Series. NACA RM L52L18, 1953.

3. Wiggins, James W., and Fournier, Paul G.: Wind-Tunnel Investigation of the Static Lateral Stability Characteristics of Wing-Fuselage Combinations at High Subsonic Speeds - Taper-Ratio Series. NACA RM L53B25a, 1953.

4. Kuhn, Richard E., and Draper, John W.: Wind-Tunnel Investigation of the Effects of Geometric Dihedral on the Aerodynamic Characteristics in Pitch and Sideslip of an Unswept- and a 45° Sweptback-Wing-Fuselage Combination at High Subsonic Speeds. NACA RM L53F09, 1953.

5. Wiggins, James W.: Wind-Tunnel Investigation at High Subsonic Speeds of the Static Longitudinal and Static Lateral Stability Characteristics of a Wing-Fuselage Combination Having a Triangular Wing of Aspect Ratio 2.31 and an NACA 65A003 Airfoil. NACA RM L53G09a, 1953.

6. Fournier, Paul G.: Wind-Tunnel Investigation of the Aerodynamic Characteristics in Pitch and Sideslip at High Subsonic Speeds of a Wing-Fuselage Combination Having a Triangular Wing of Aspect Ratio 4. NACA RM L53G14a, 1953.

7. Polhamus, Edward C., and Sleeman, William C., Jr.: The Rolling Moment Due to Sideslip of Swept Wings at Subsonic and Transonic Speeds. NACA RM L54L01, 1955.

8. Gillis, Clarence L., Polhamus, Edward C., and Gray, Joseph L., Jr.: Charts for Determining Jet-Boundary Corrections for Complete Models in 7- by 10-Foot Closed Rectangular Wind Tunnels. NACA WR L-123, 1945. (Formerly NACA ARR L5G31.)

9. Herriot, John G.: Blockage Corrections for Three-Dimensional-Flow Closed-Throat Wind Tunnels, With Consideration of the Effect of Compressibility. NACA Rep. 995, 1950. (Supersedes NACA RM A7B28.)

10. Nielsen, Jack N., Kaattari, George E., and Anastasio, Robert F.: A Method for Calculating the Lift and Center of Pressure of Wing-Body-Tail Combinations at Subsonic, Transonic, and Supersonic Speeds. NACA RM A53G08, 1953.

11. Göthert, B.: Airfoil Measurements in the DVL High-Speed Wind Tunnel (2.7-Meter Diameter). NACA TM 1240, 1949.

12. Daley, Bernard N., and Dick, Richard S.: Effect of Thickness, Camber, and Thickness Distribution on Airfoil Characteristics at Mach Numbers Up to 1.0. NACA TN 3607, 1956. (Supersedes NACA RM L52G31a.)

13. Lomax, Harvard, and Sluder, Loma: Chordwise and Compressibility Corrections to Slender-Wing Theory. NACA Rep. 1105, 1952. (Supersedes NACA TN 2295.)

14. Falkner, V. M. (With Appendix by Doris Lehrian): Calculated Loadings Due to Incidence of a Number of Straight and Swept-Back Wings. R. & M. No. 2596, British A.R.C., June 1948.

15. Abbott, Ira H., von Doenhoff, Albert E., and Stivers, Louis S., Jr.: Summary of Airfoil Data. NACA Rep. 824, 1945. (Supersedes NACA WR L-560.)

16. Polhamus, Edward C.: Drag Due to Lift at Mach Numbers Up to 2.0. NACA RM L53I22b, 1953.

17. Boyd, John W., Migotsky, Eugene, and Wetzel, Benton E.: A Study of Conical Camber for Triangular and Sweptback Wings. NACA RM A55G19, 1955.

18. Polhamus, Edward C., and Hallissy, Joseph M., Jr.: Effect of Airplane Configuration on Static Stability at Subsonic and Transonic Speeds. NACA RM L56A09a, 1956.

[redacted]

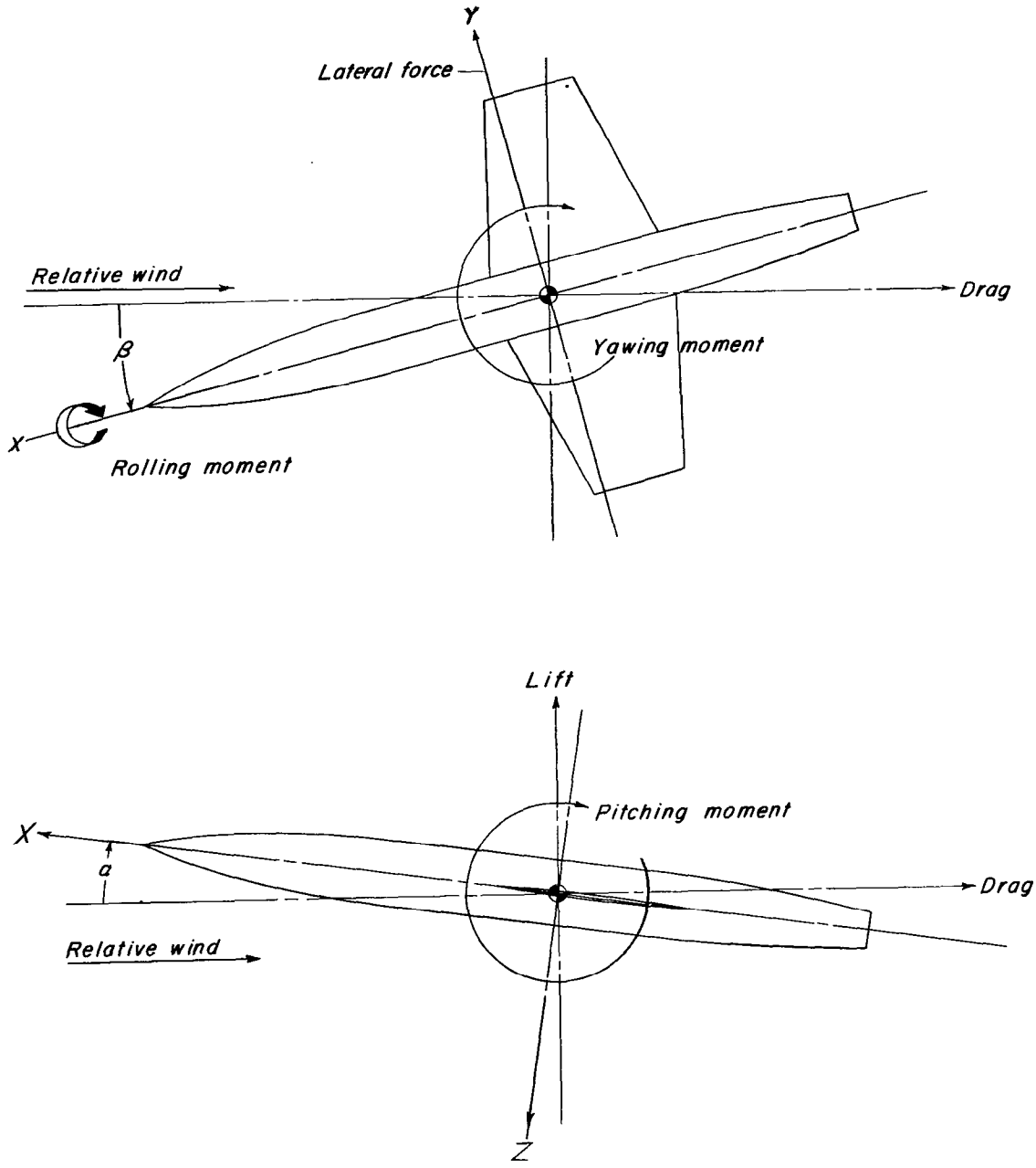

Figure 1.- System of axes. Arrows indicate positive directions of forces, moments, and angles.

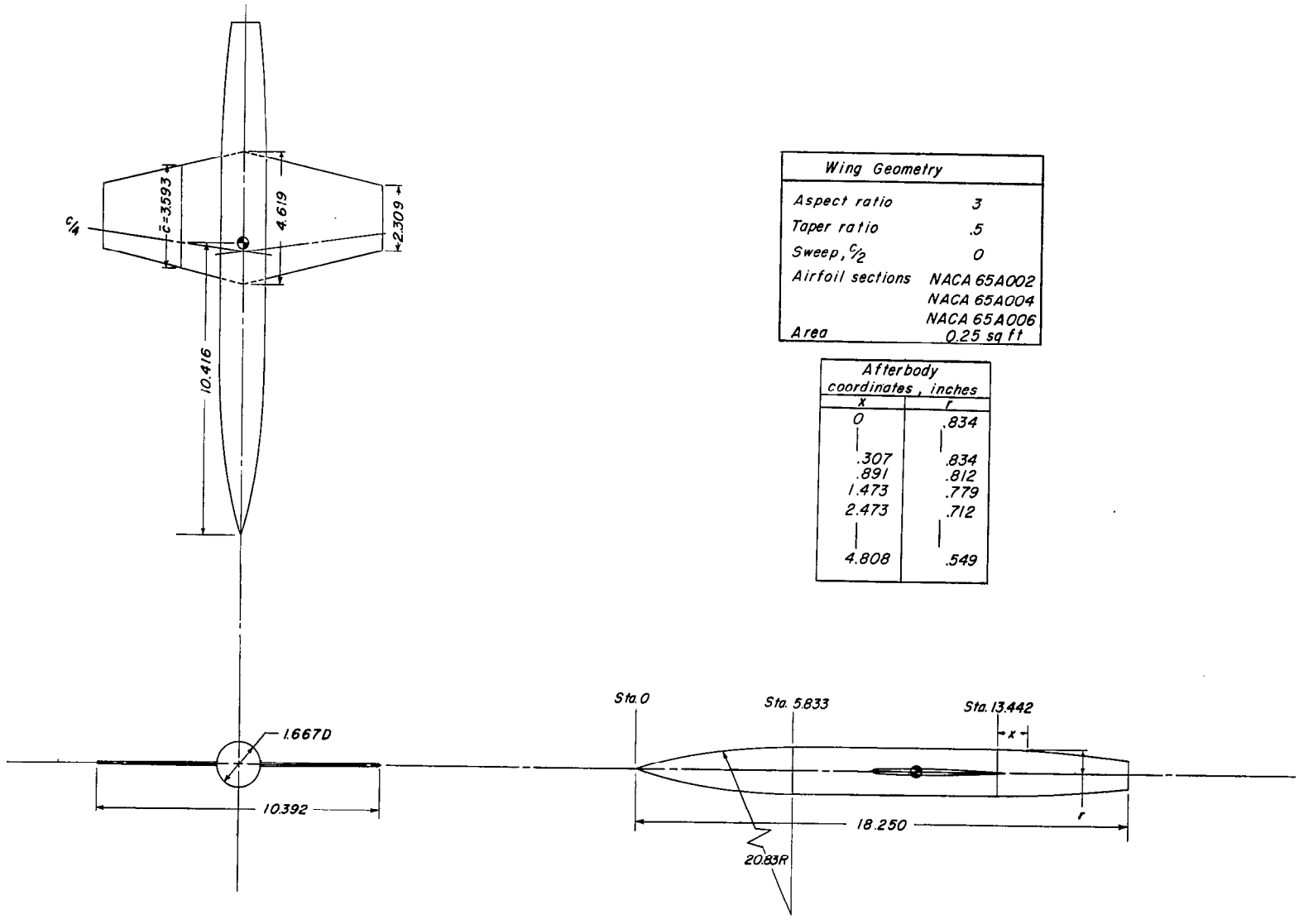

Wing Geometry	
Aspect ratio	3
Taper ratio	.5
Sweep, $c/2$	0
Airfoil sections	NACA 65A002 NACA 65A004 NACA 65A006
Area	0.25 sq ft

Afterbody coordinates, inches	
x	r
0	.834
.307	.834
.891	.812
1.473	.779
2.473	.712
4.808	.549

Figure 2.- Details of complete model. All dimensions are in inches.

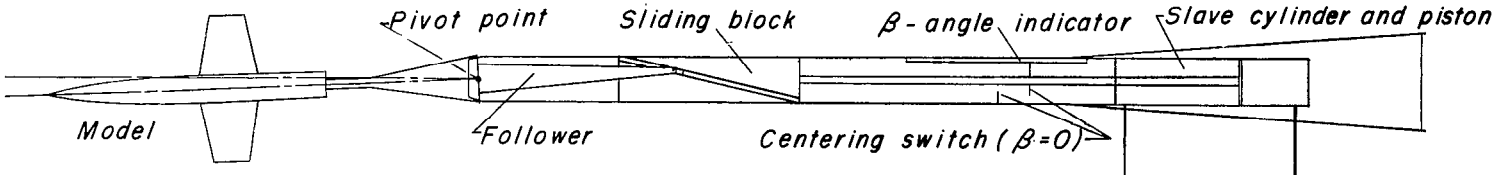

(a) Variable-yaw sting.

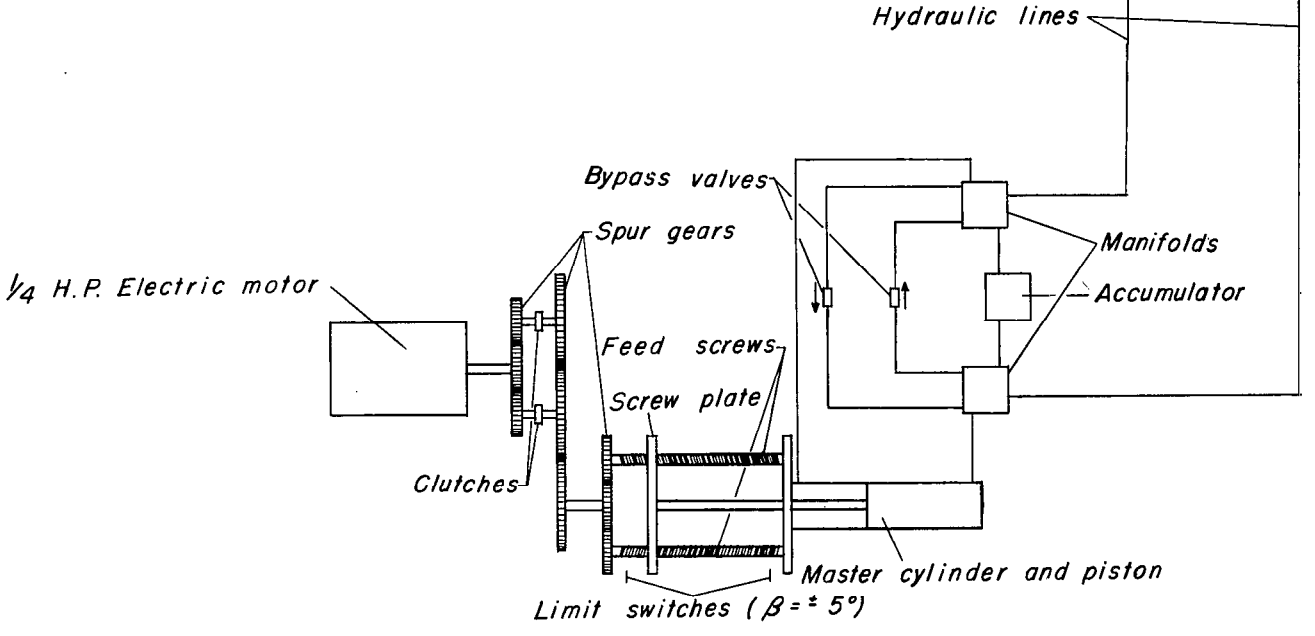

(b) Actuating mechanism.

Figure 3.- Variable-yaw mechanism.

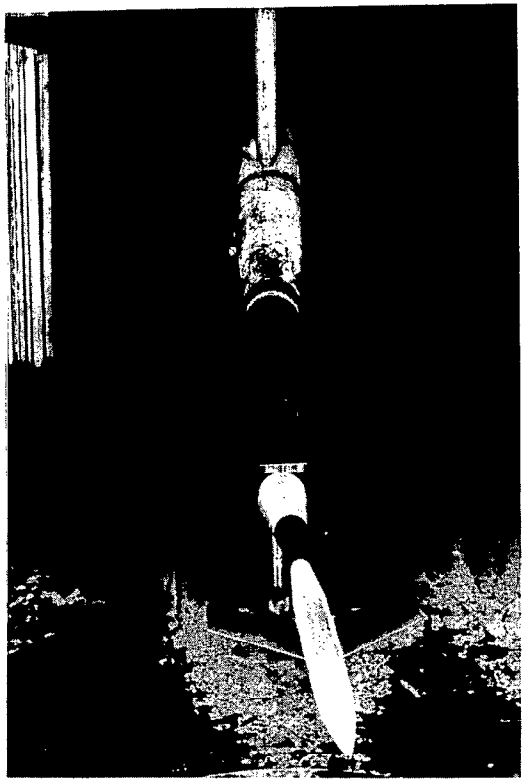

Variable-yaw sting mounted in tunnel.

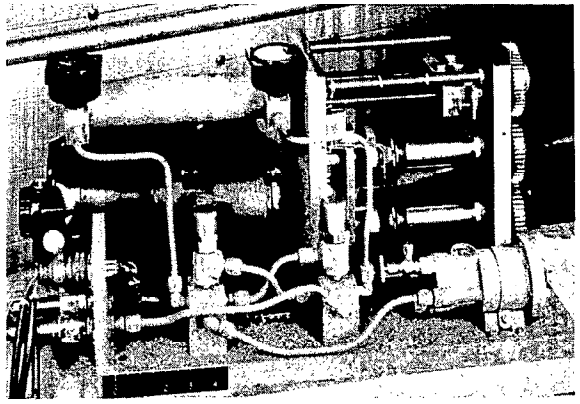

Actuating mechanism - left side.

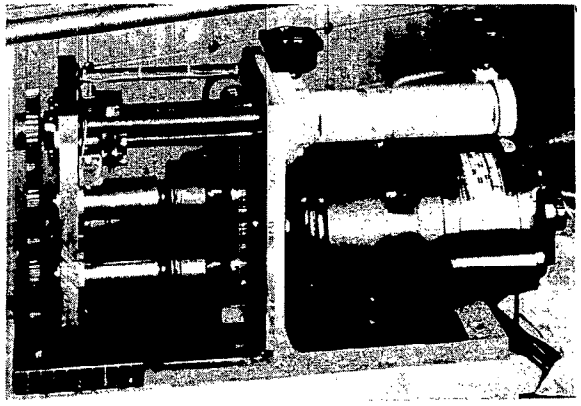

Actuating mechanism - right side.

(c) Photographs of variable-yaw apparatus. L-93524

Figure 3.- Concluded.

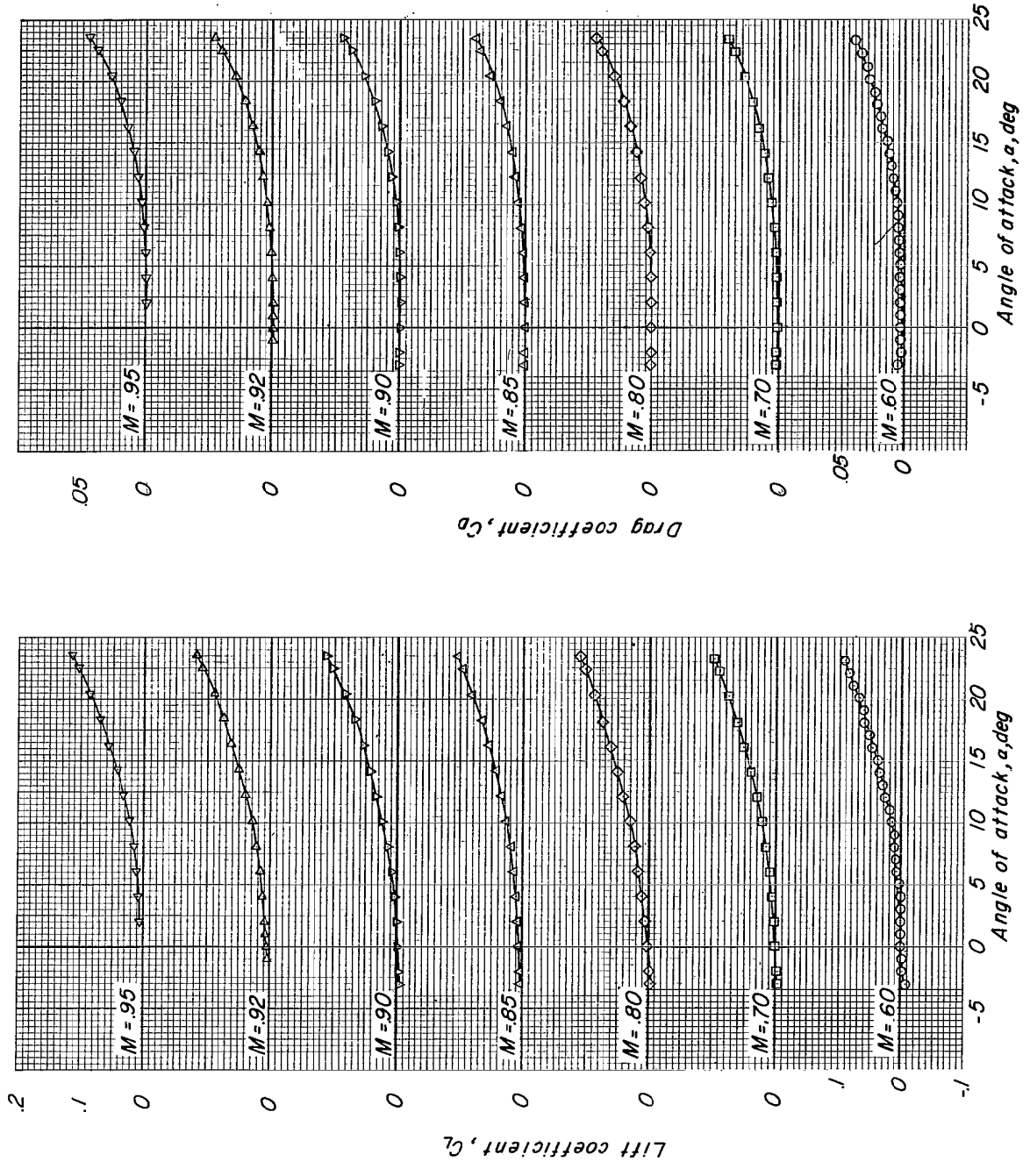

Figure 4.- Longitudinal stability characteristics of fuselage alone.

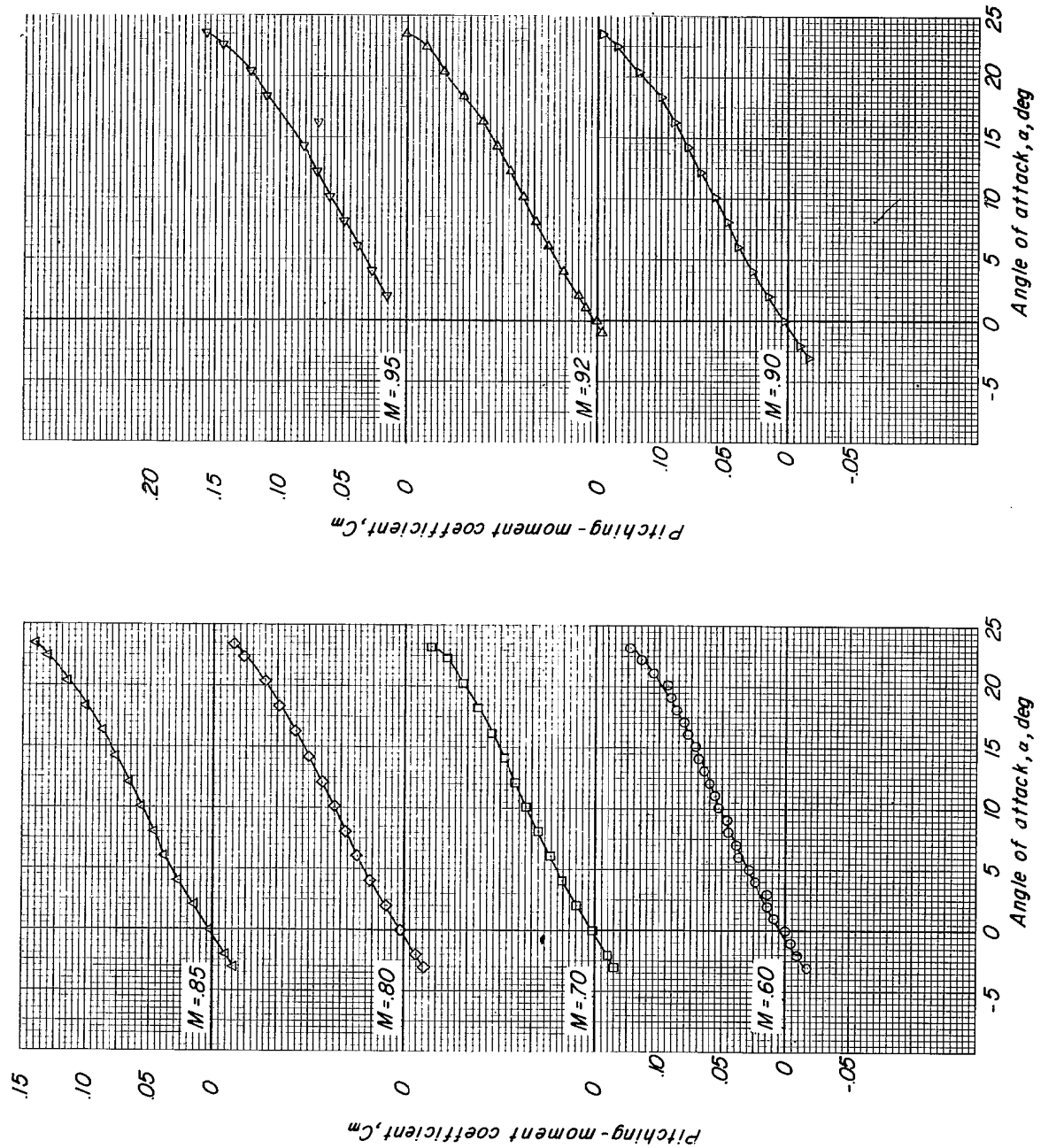

Figure 4.- Concluded.

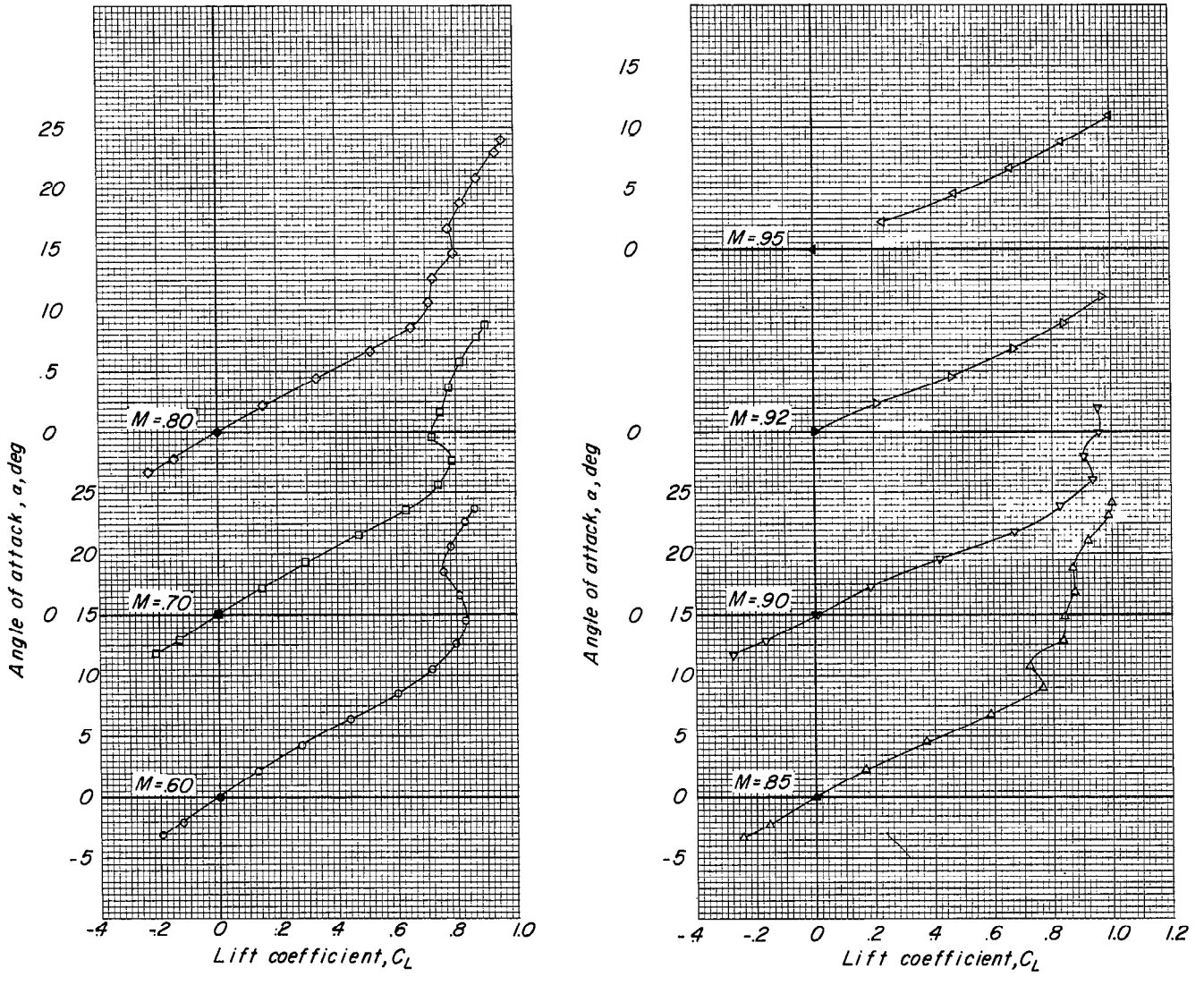

(a) t/c = 0.02.

Figure 5.- Variation of angle of attack with lift coefficient for wing-fuselage combinations. Solid symbols indicate origins of axes.

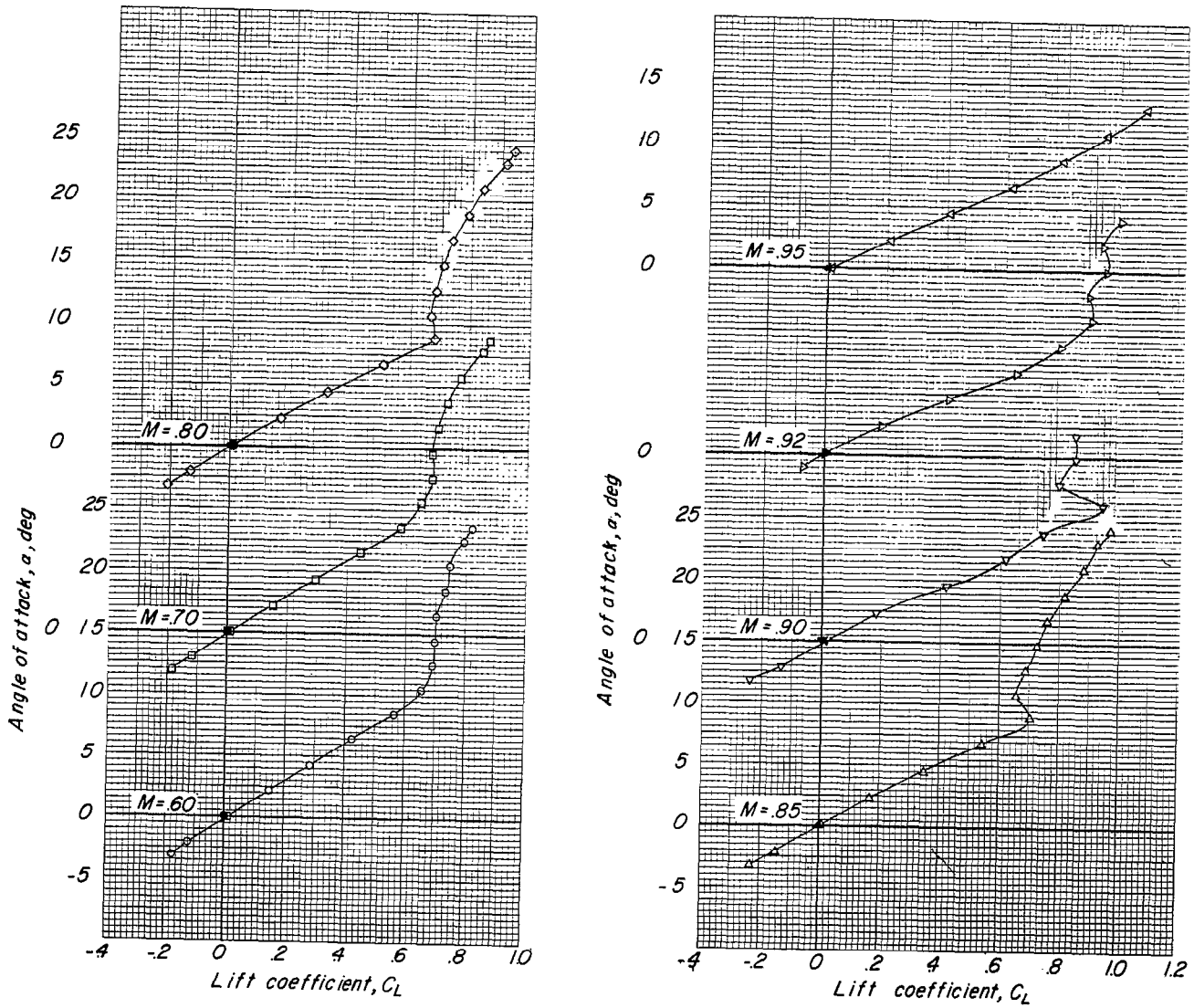

(b) t/c = 0.04.

Figure 5.- Continued.

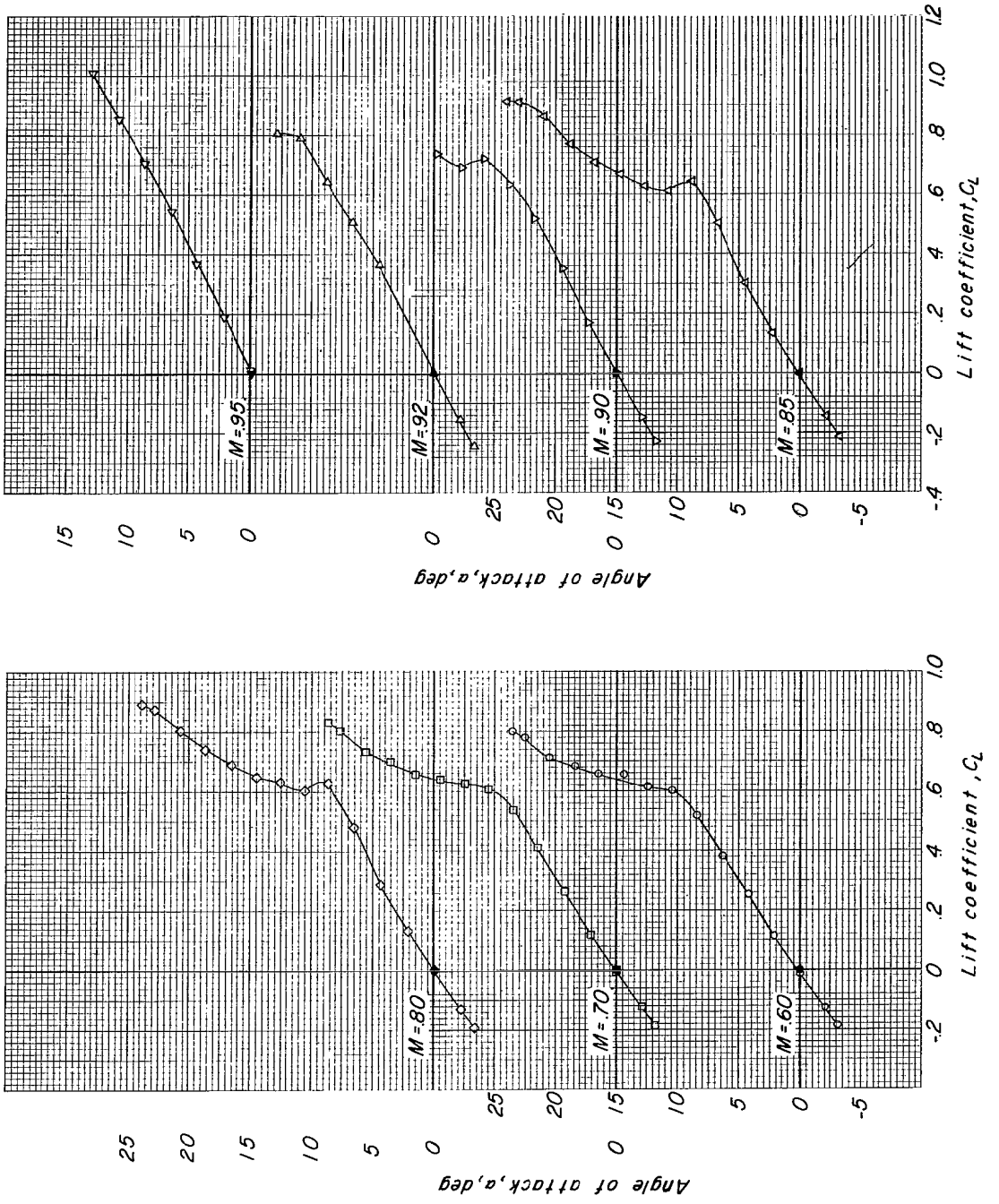

(c) t/c = 0.06.

Figure 5.- Concluded.

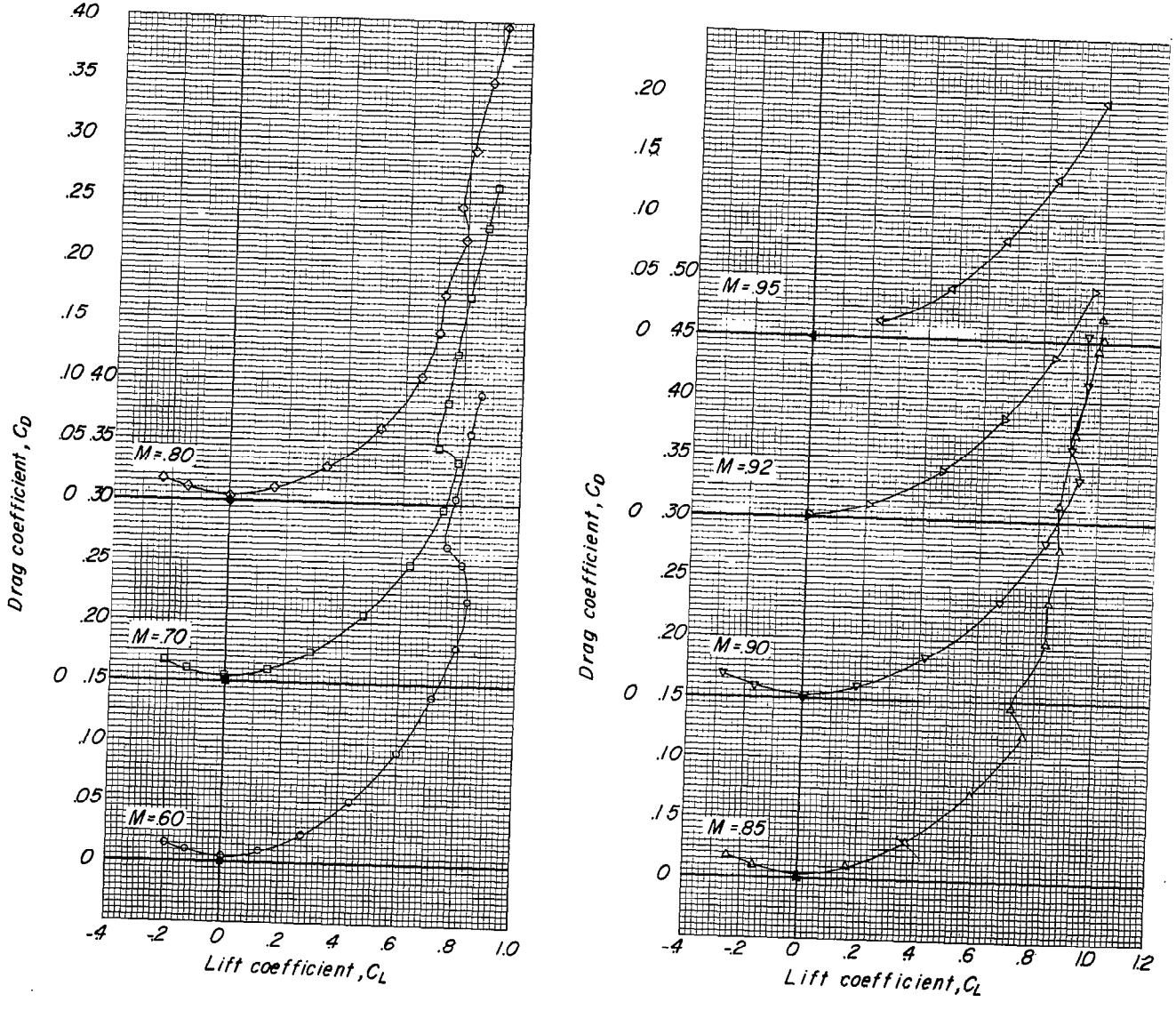

(a) t/c = 0.02.

Figure 6.- Variation of drag coefficient with lift coefficient for wing-fuselage combinations. Solid symbols indicate origins of axes.

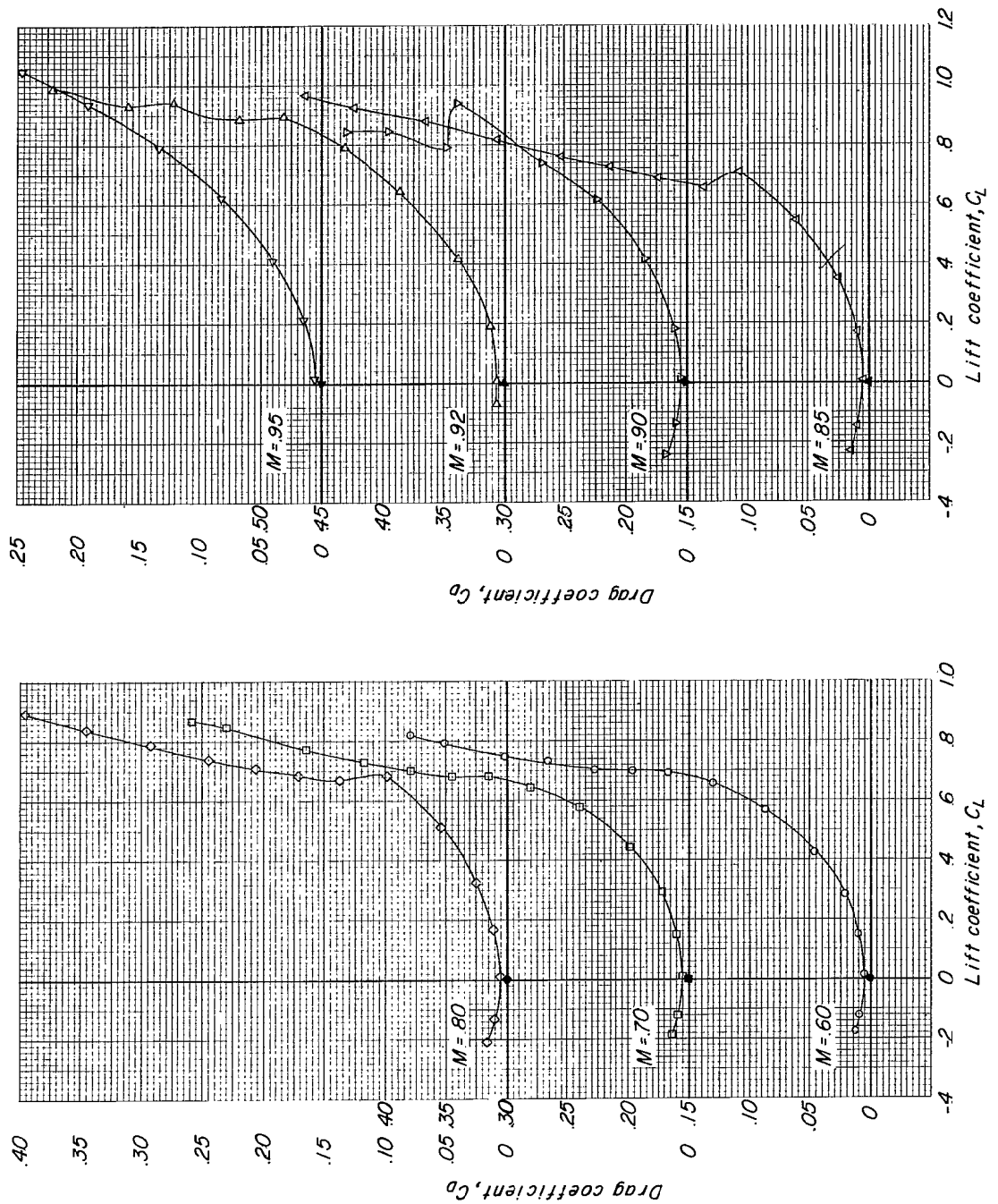

(b) t/c = 0.04.

Figure 6.- Continued.

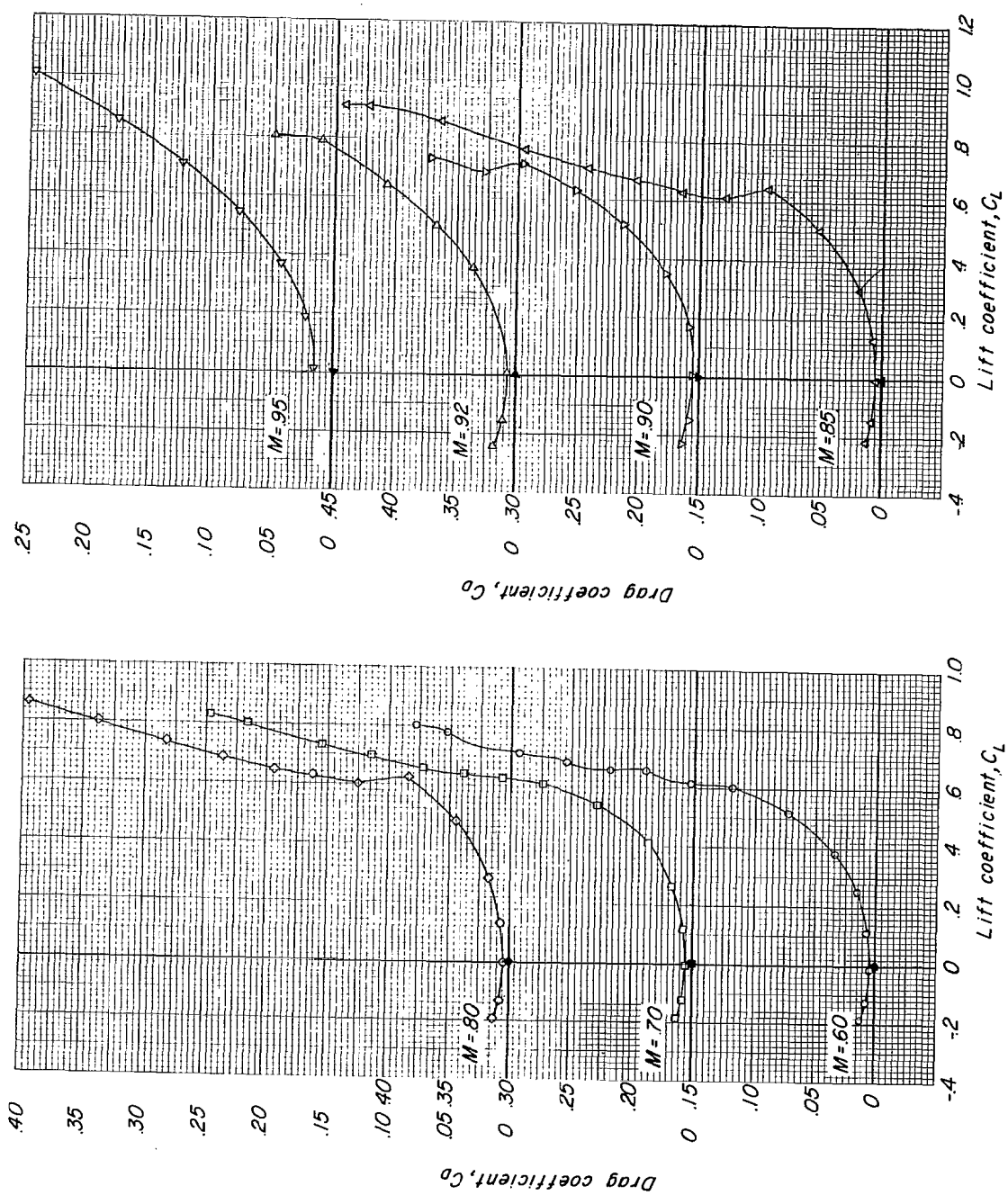

(c) t/c = 0.06.

Figure 6.- Concluded.

[redacted]

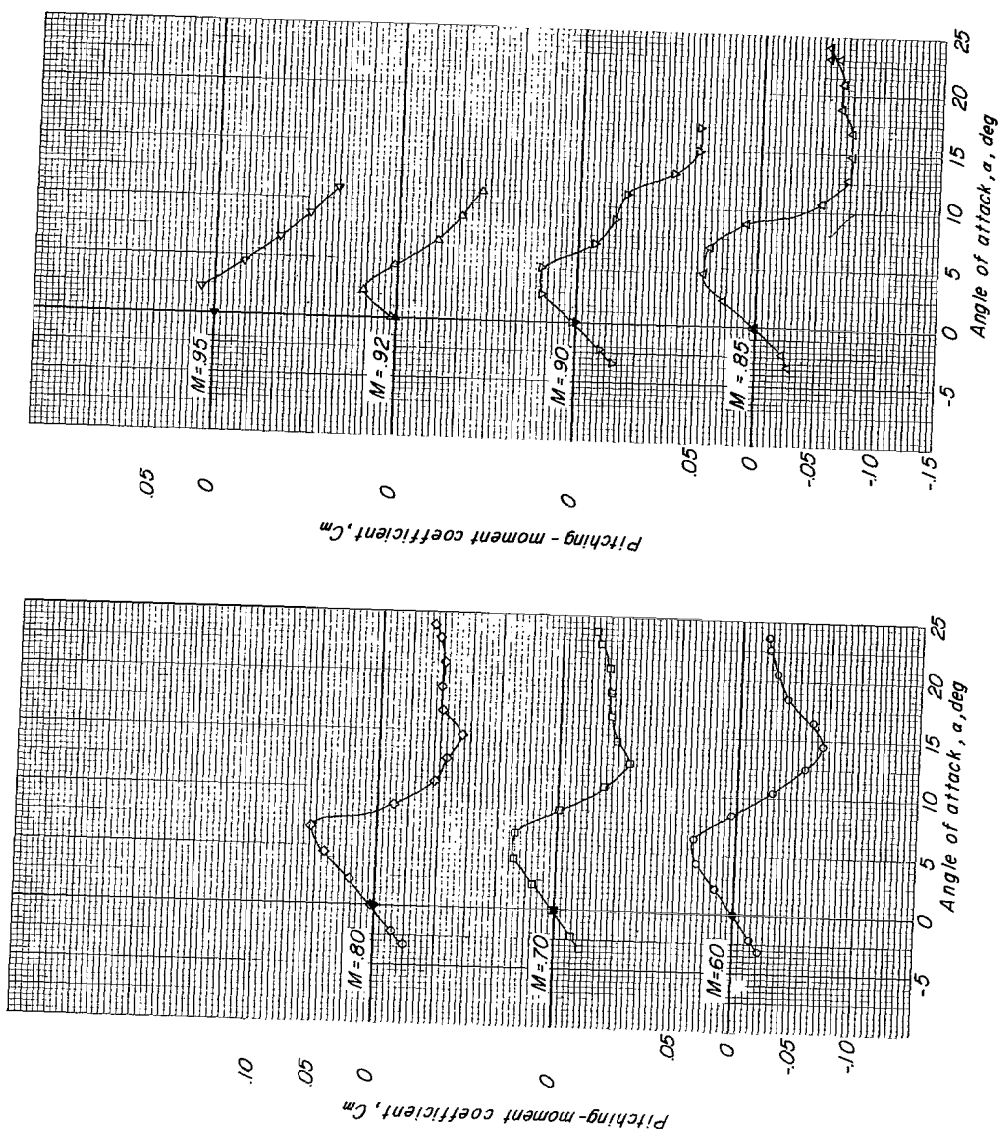

(a) t/c = 0.02.

Figure 7.- Variation of pitching-moment coefficient with angle of attack for wing-fuselage combinations. Solid symbols indicate origins of axes.

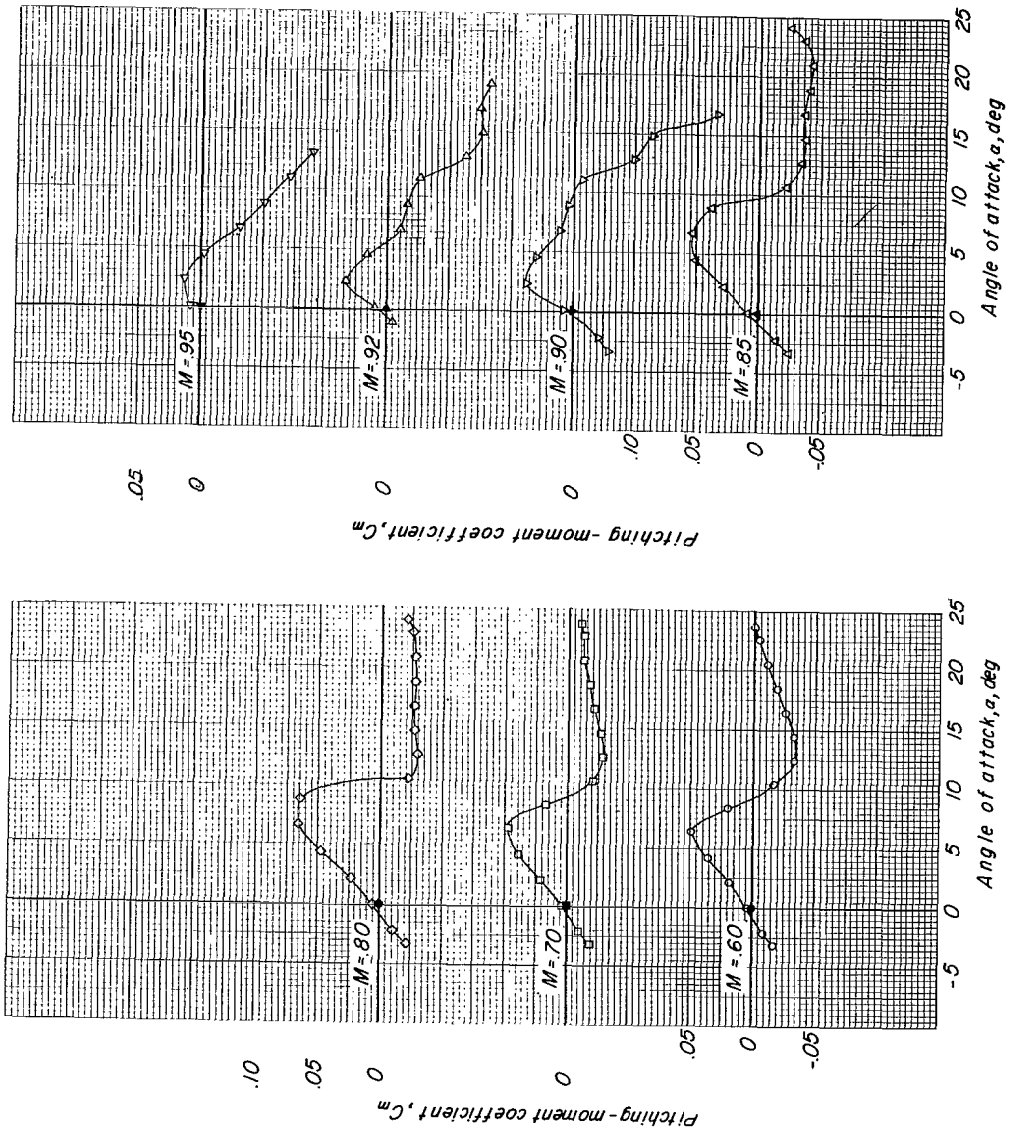

(b) t/c = 0.04.

Figure 7.- Continued.

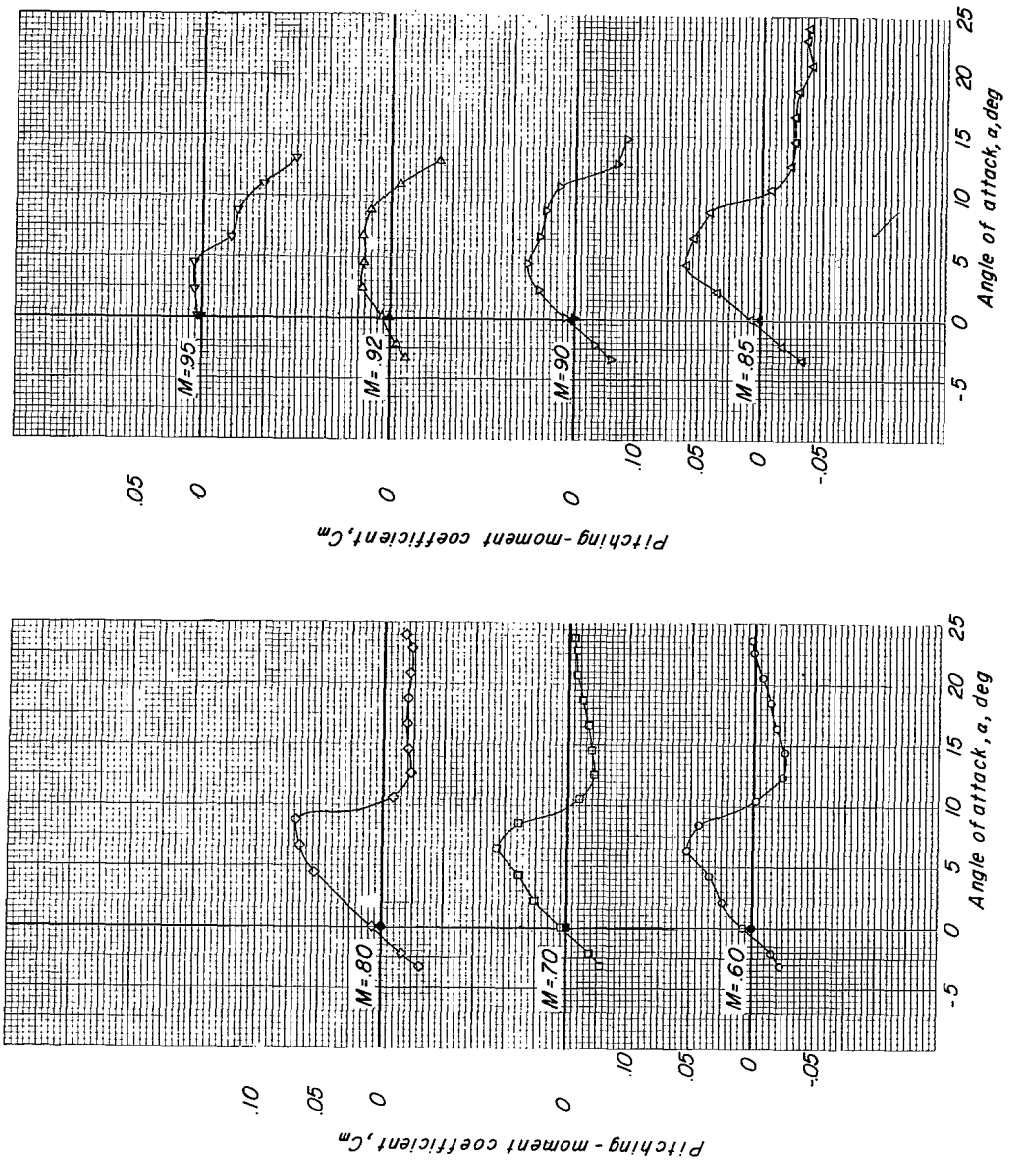

(c) t/c = 0.06.

Figure 7.- Concluded.

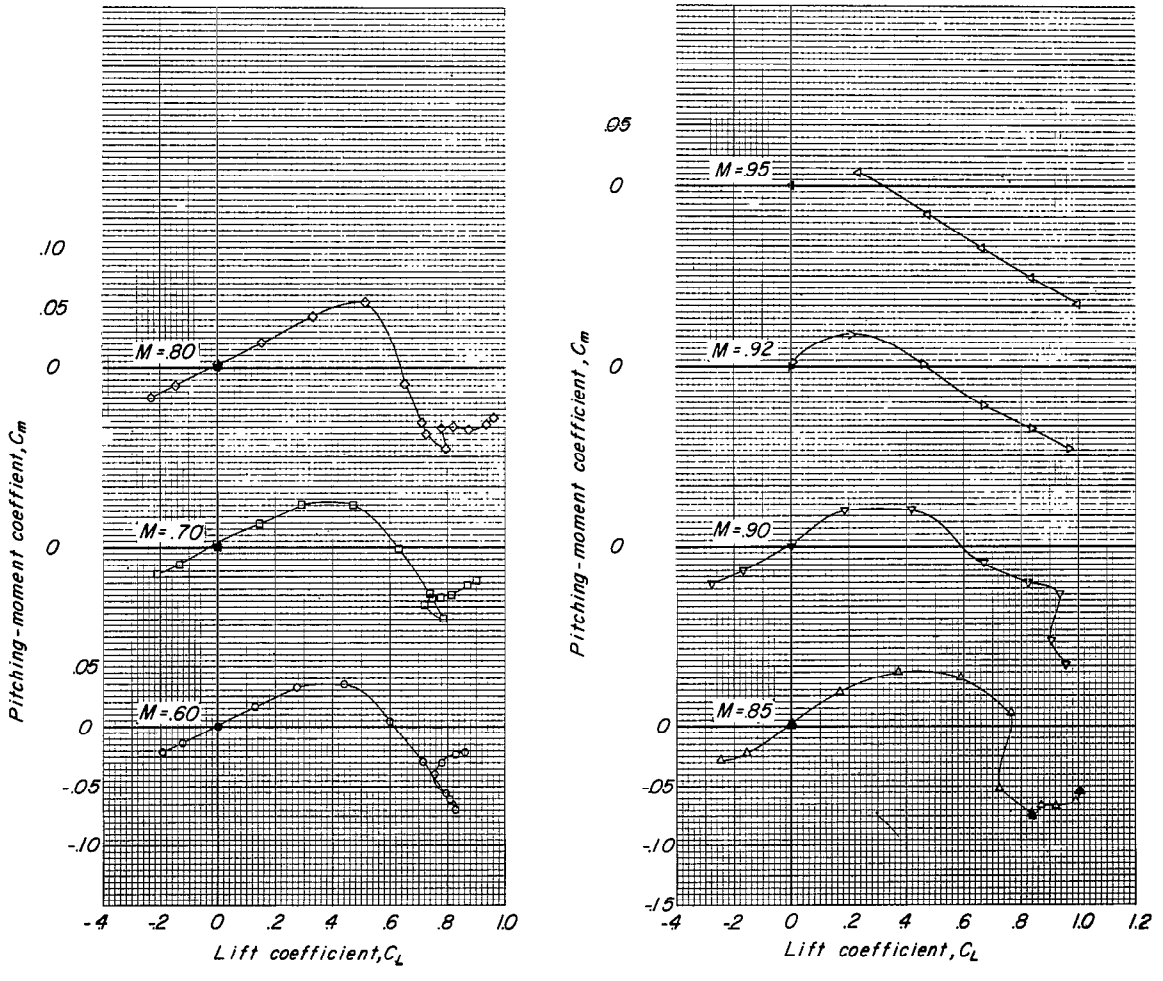

(a) t/c = 0.02.

Figure 8.- Variation of pitching-moment coefficient with lift coefficient for wing-fuselage combinations. Solid symbols indicate origins of axes.

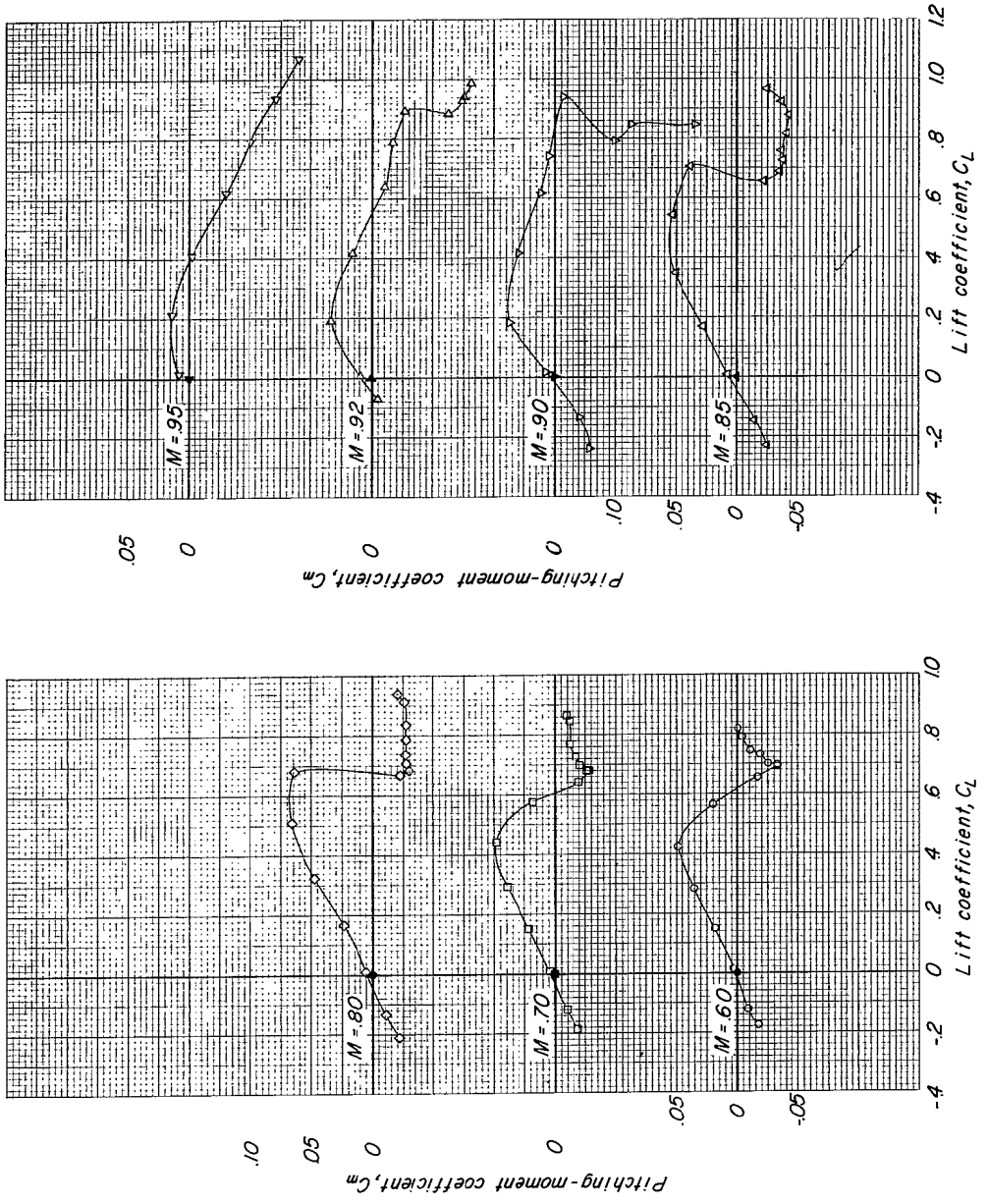

(b) t/c = 0.04.

Figure 8.- Continued.

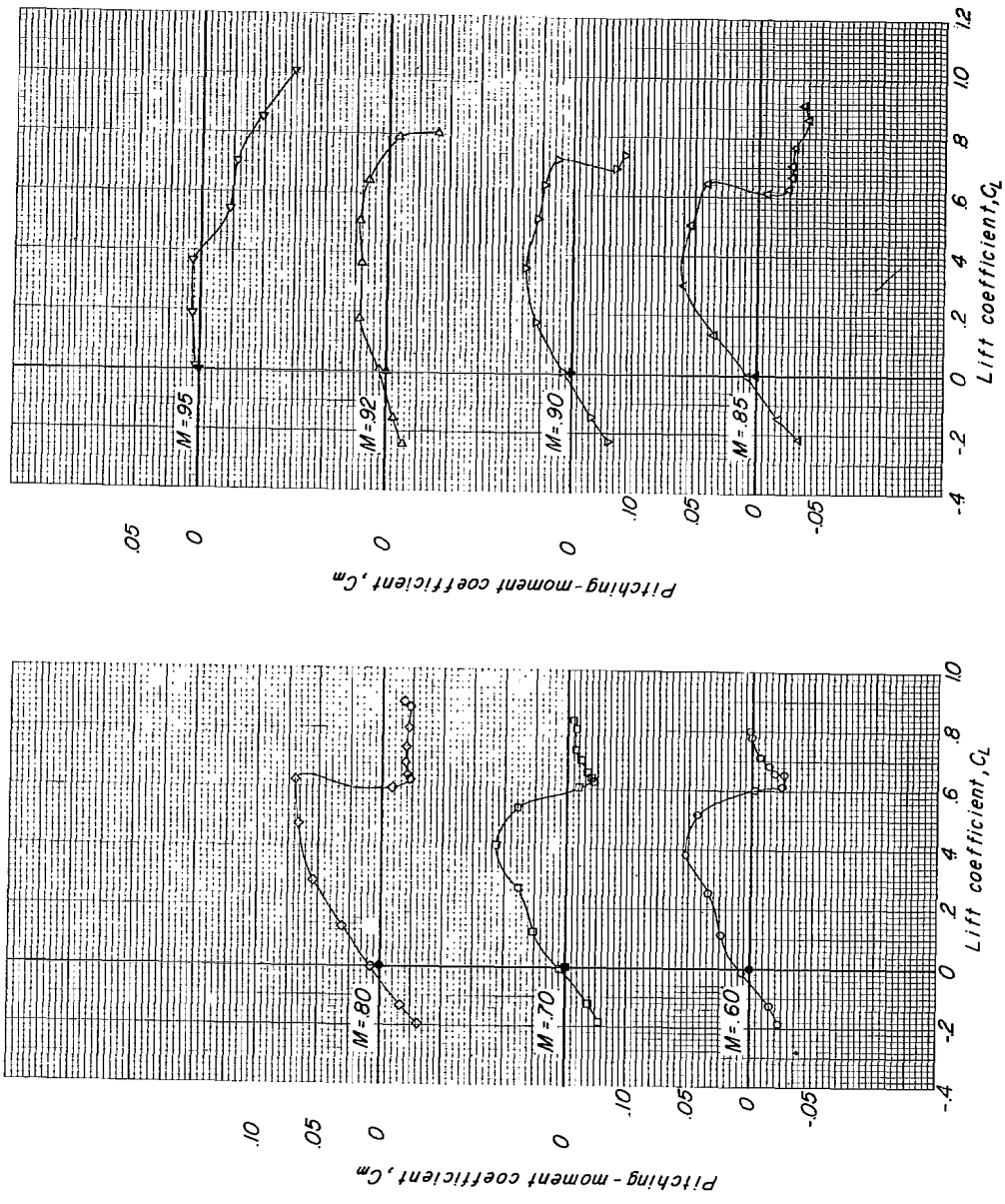

(c) t/c = 0.06.

Figure 8.- Concluded.

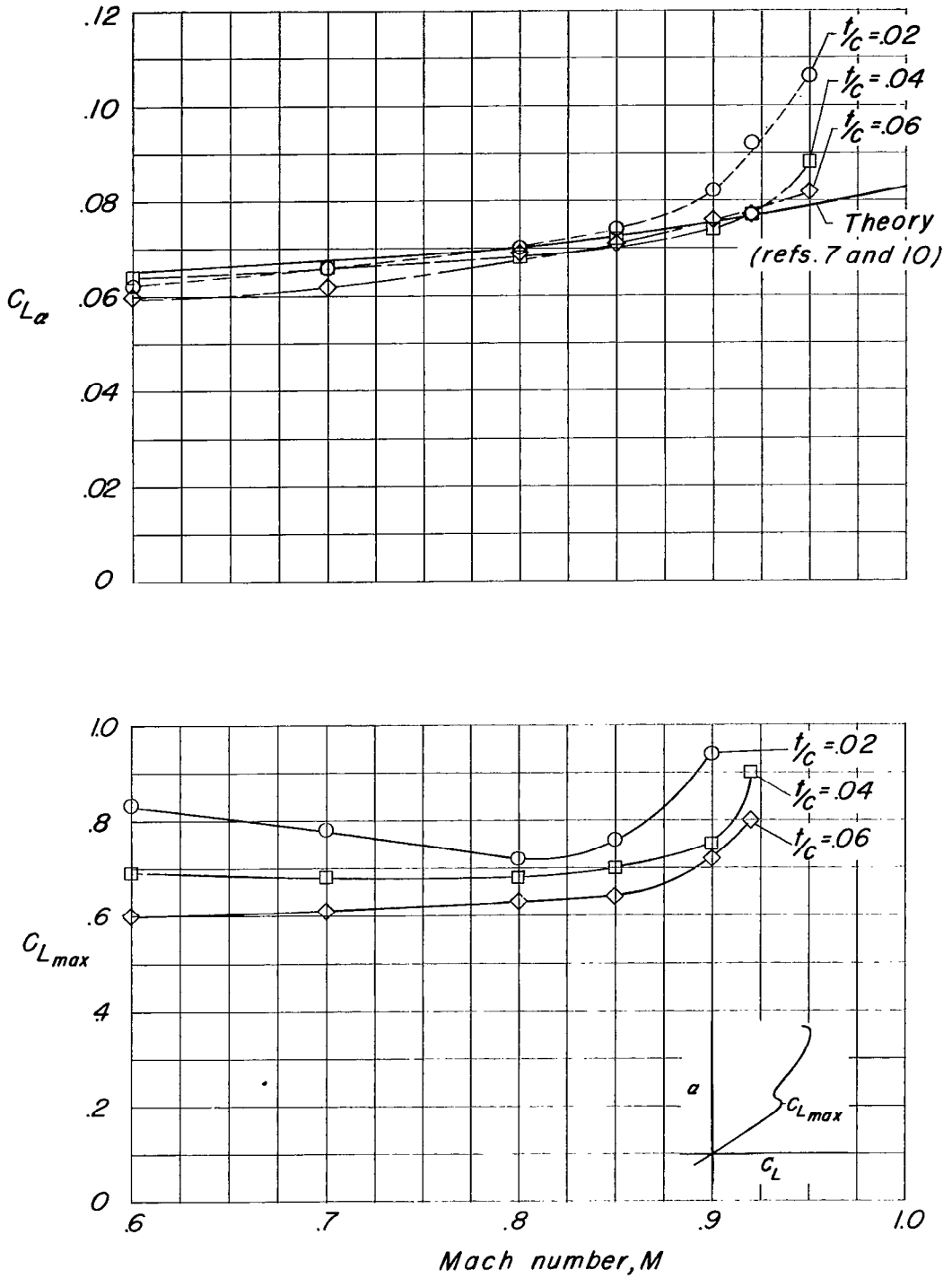

Figure 9.- Variation of lift-curve slope and maximum lift coefficient with Mach number.

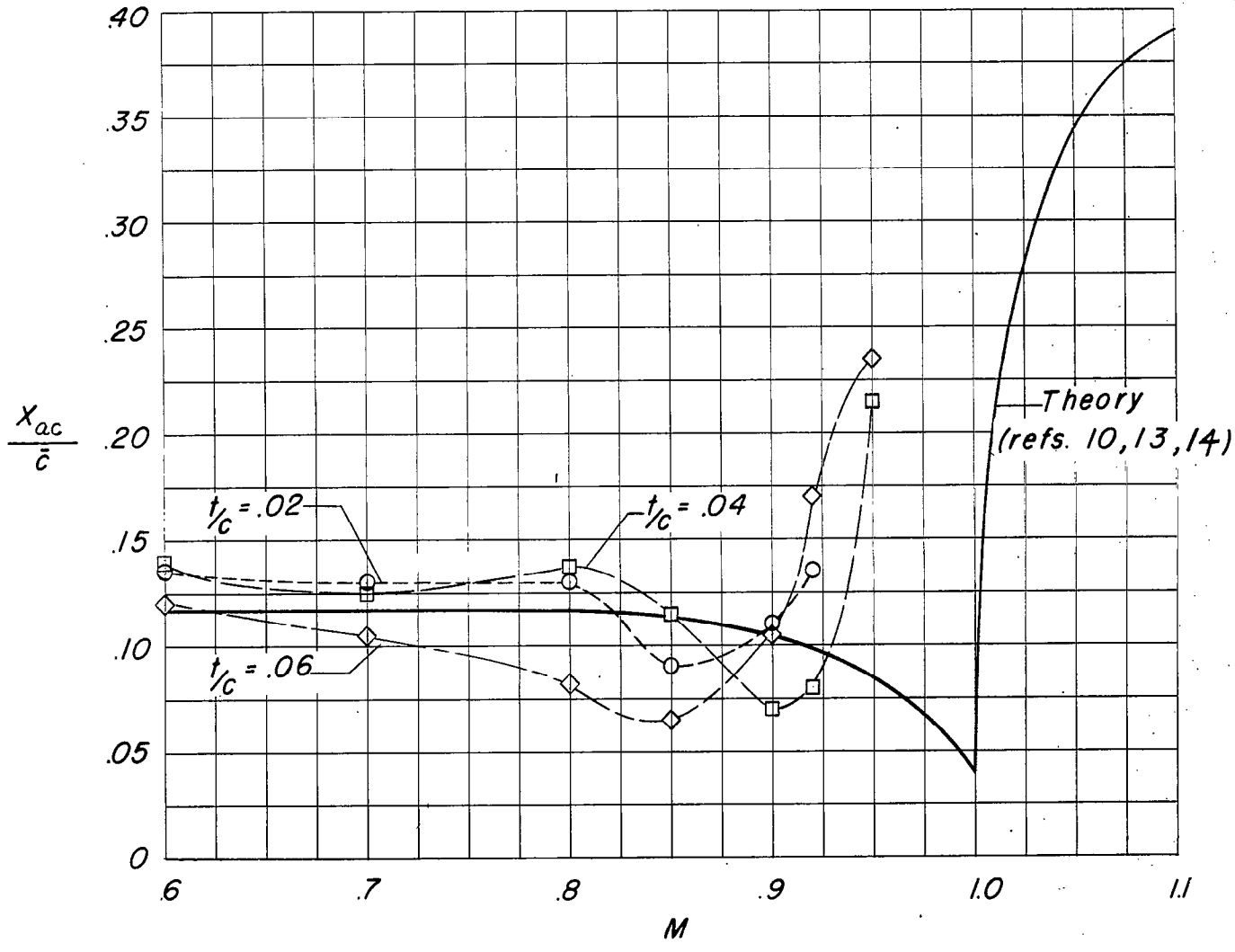

Figure 10.- Comparison of theory with experimental variation of aerodynamic center.

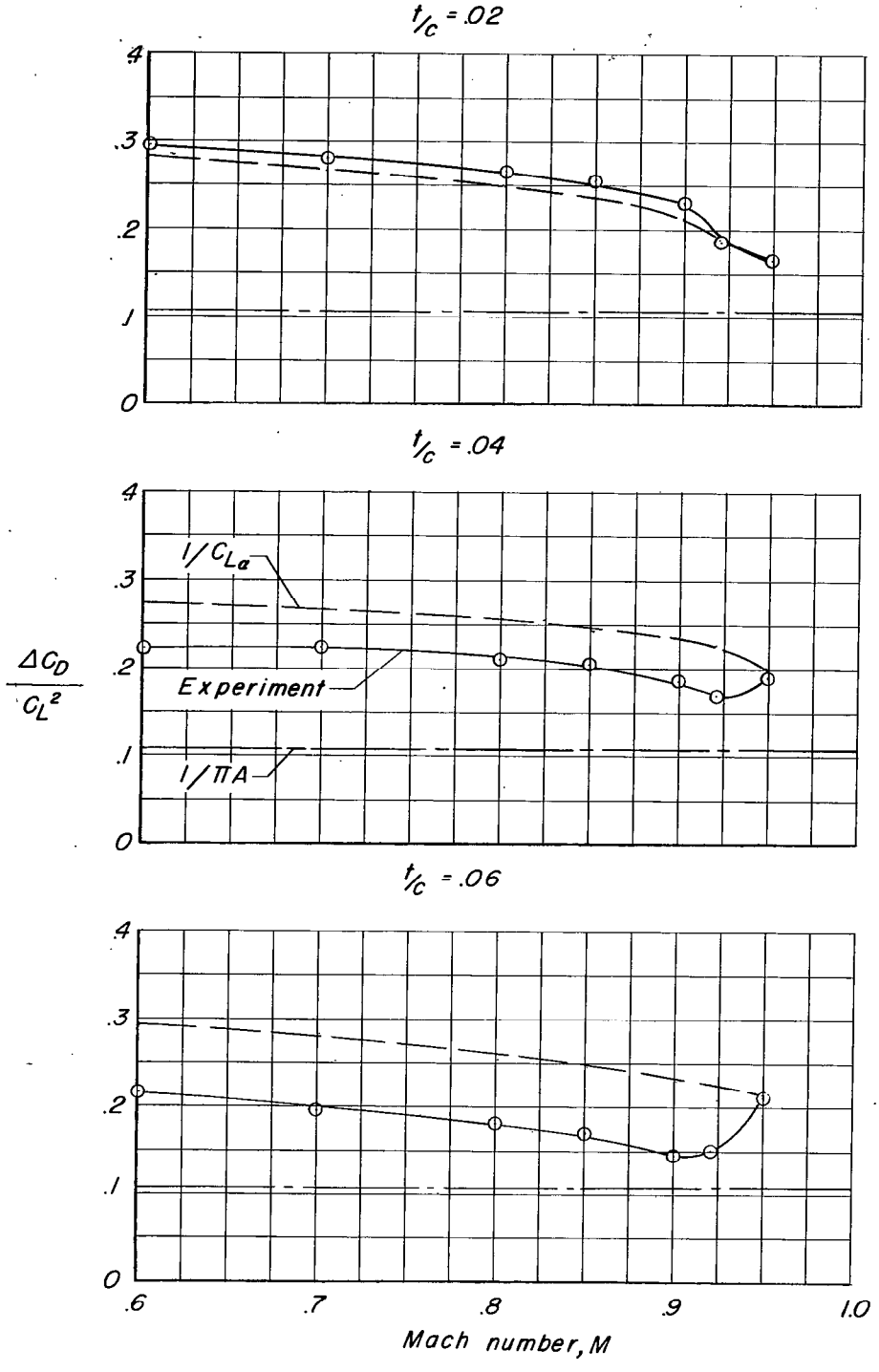

Figure 11.- The effect of Mach number on drag due to lift.

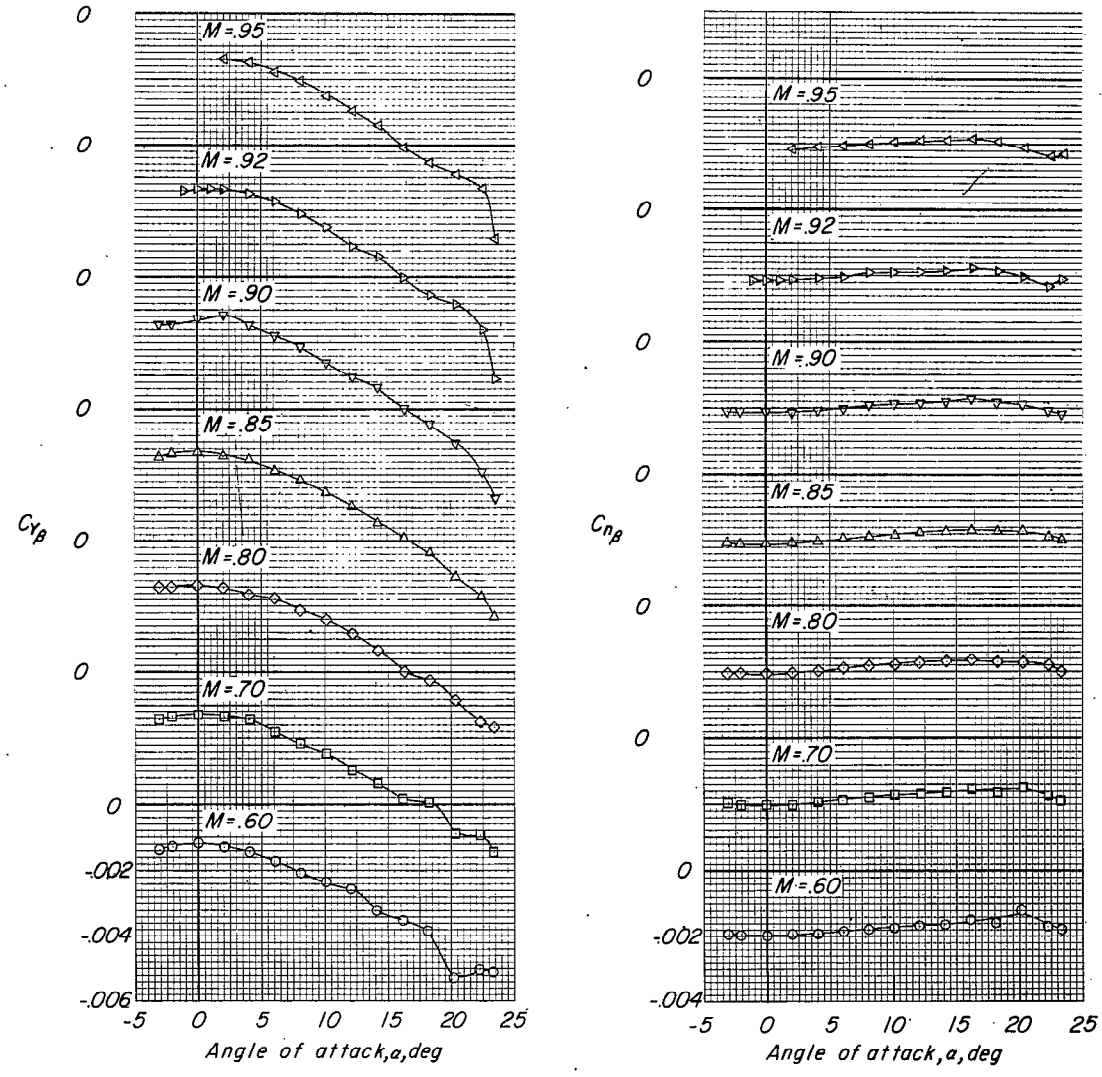

Figure 12.- Lateral stability characteristics of fuselage alone.

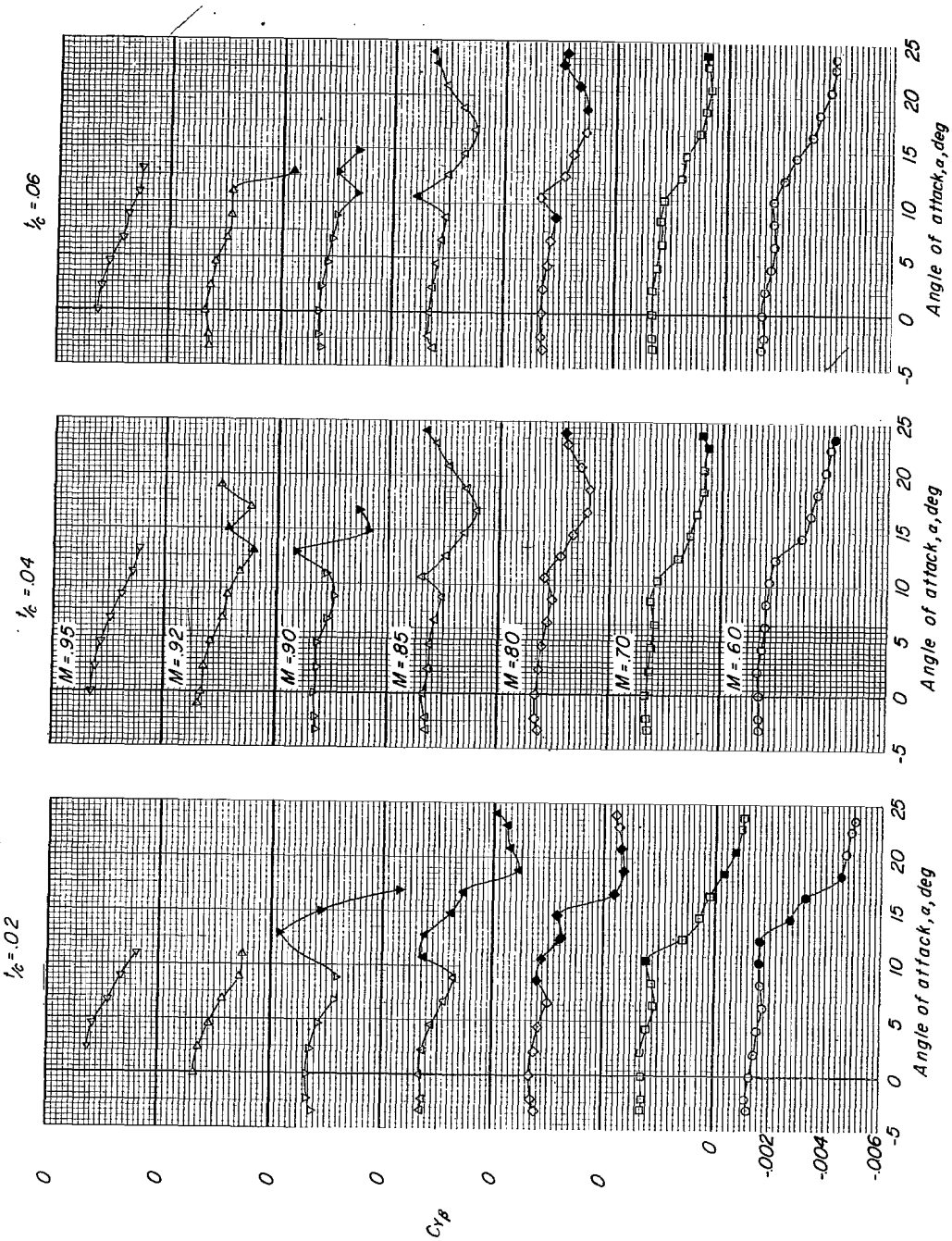

Figure 13.- Variation of C_{Y_β} with α for wing-fuselage combinations. Solid symbols indicate nonlinear variations of C_Y with β.

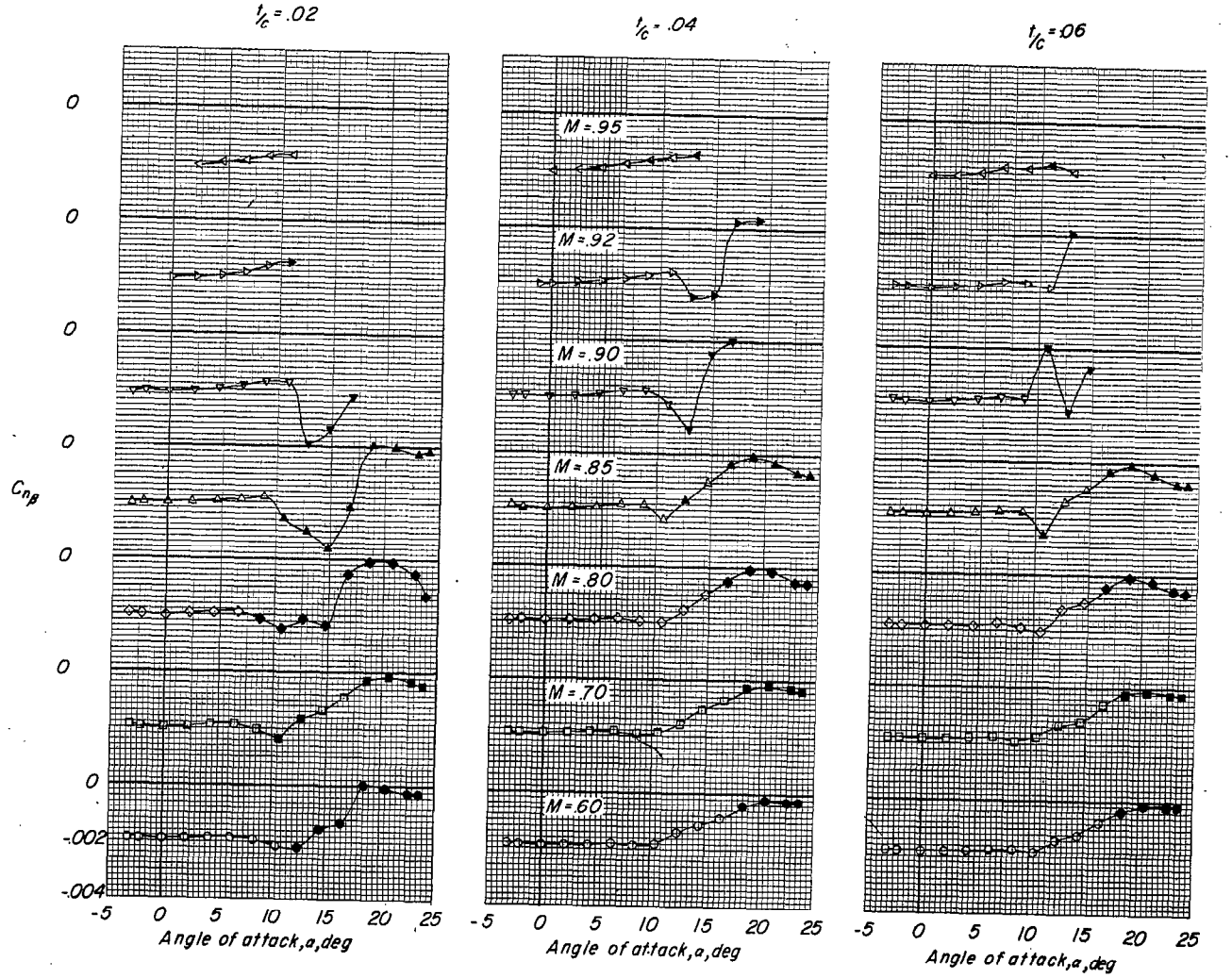

Figure 14.- Variation of C_{n_β} with α for wing-fuselage combinations. Solid symbols indicate nonlinear variations of C_n with β.

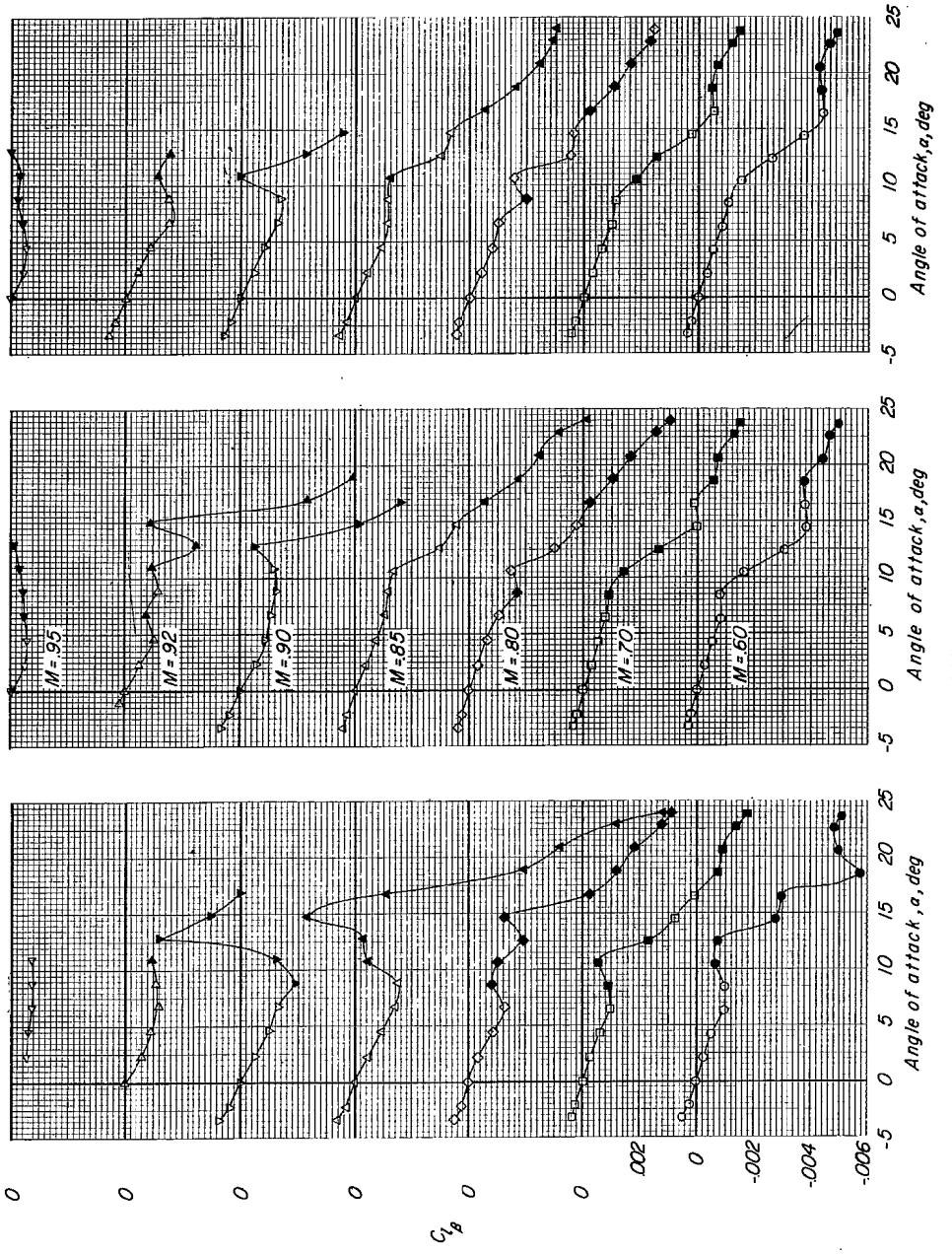

Figure 15.- Variation of C_{l_β} with α for wing-fuselage combinations. Solid symbols indicate nonlinear variations of C_l with β.

[redacted]

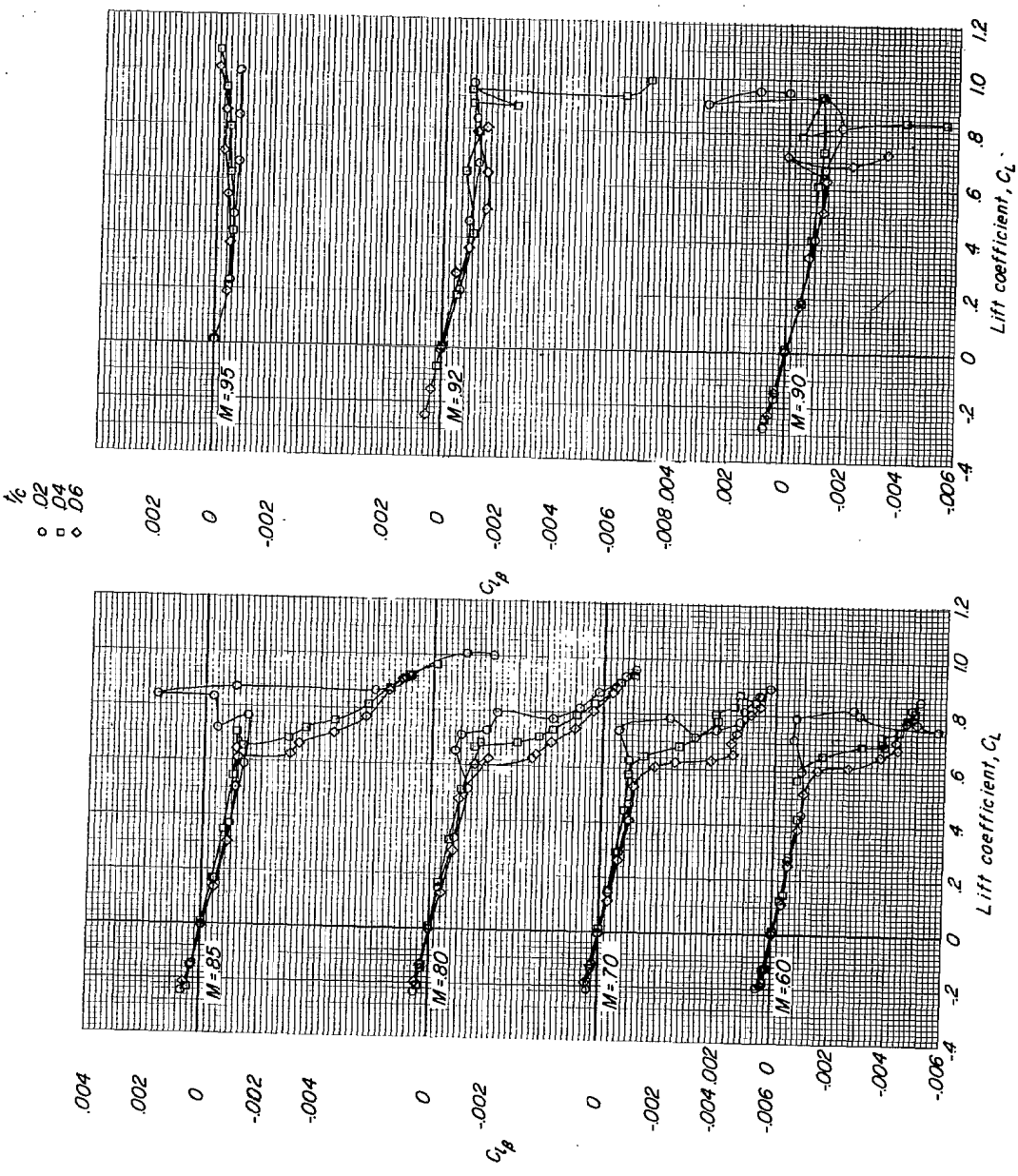

Figure 16.- Variation of effective dihedral parameter with lift coefficient.

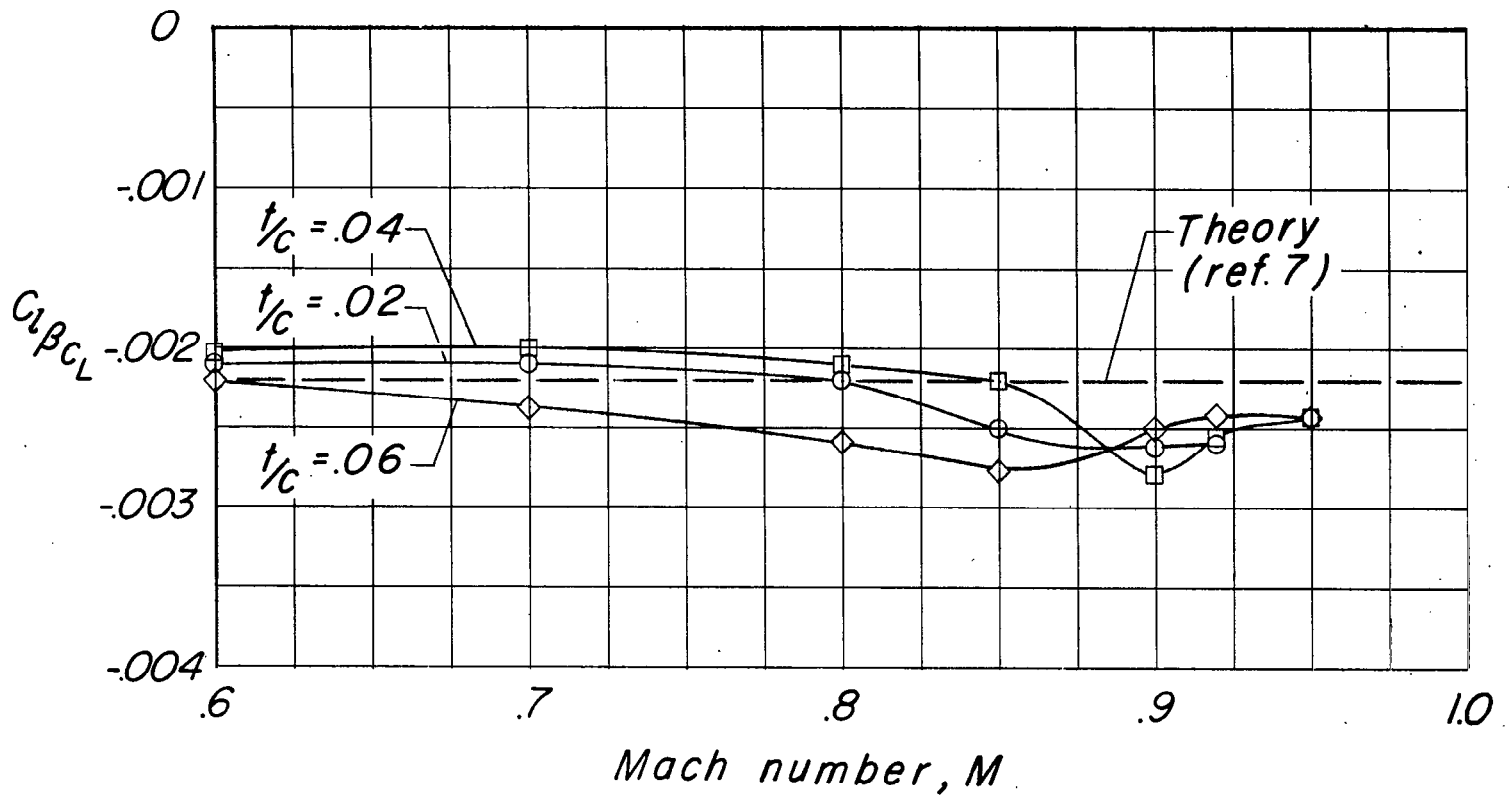

Figure 17.- The effect of Mach number on $C_{l_{\beta_{C_L}}}$.

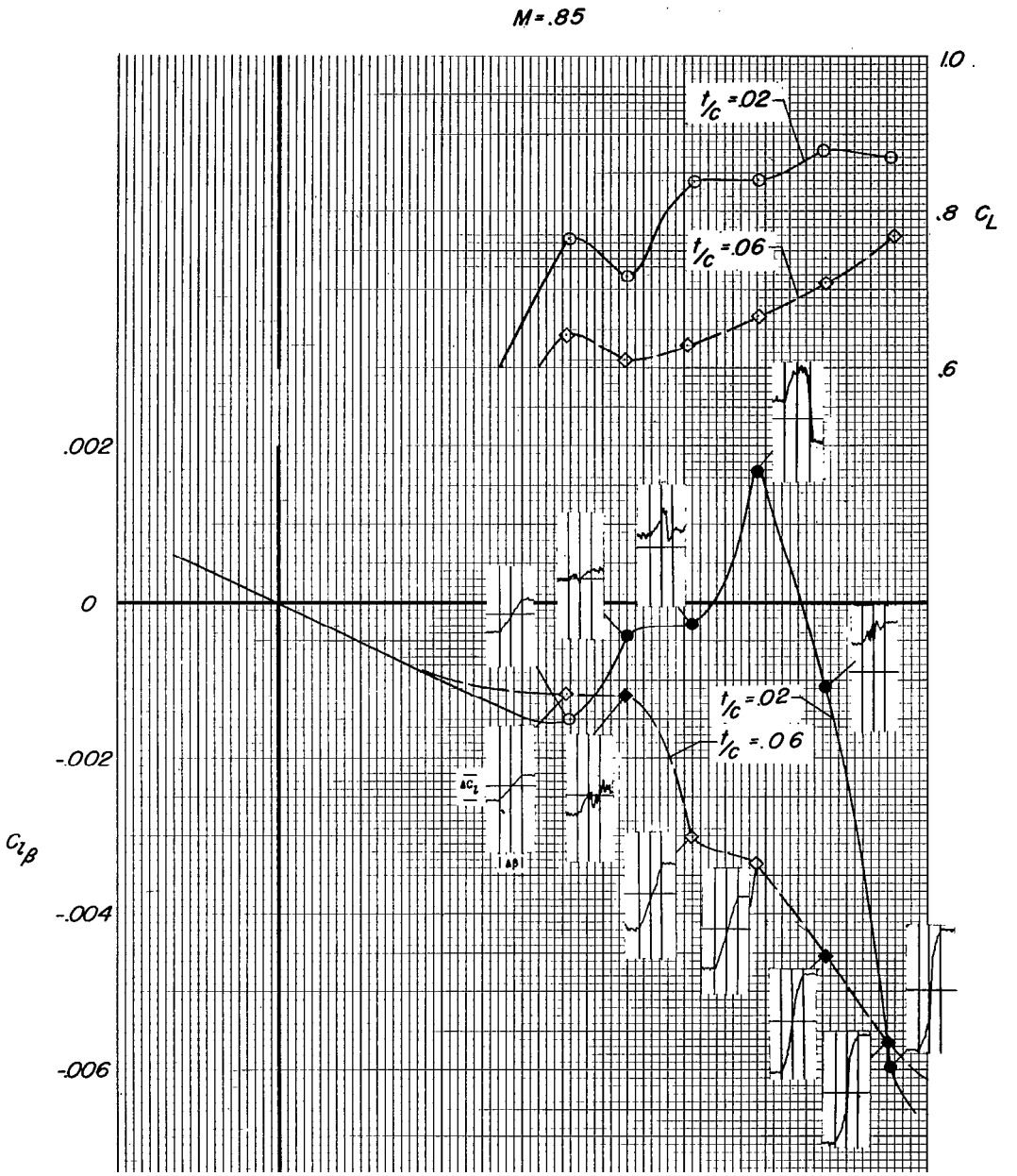
M=.85
1.0
.8
C_L
.6
t/c =.02
t/c =.06
.002
0
-.002
-.004
-.006
C_{l_β}
t/c =.02
t/c =.06

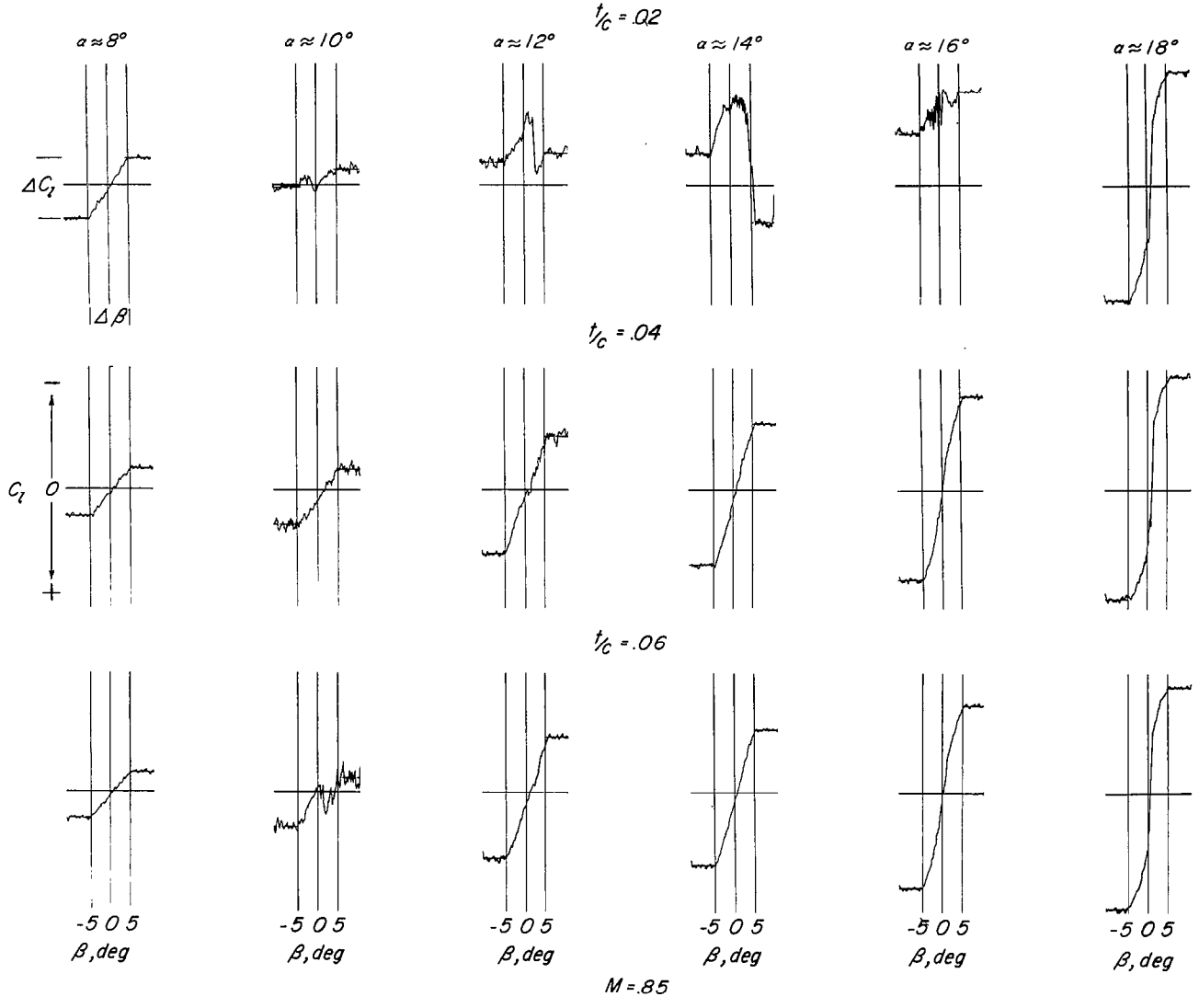

Figure 19.- Typical variations of C_l with β.

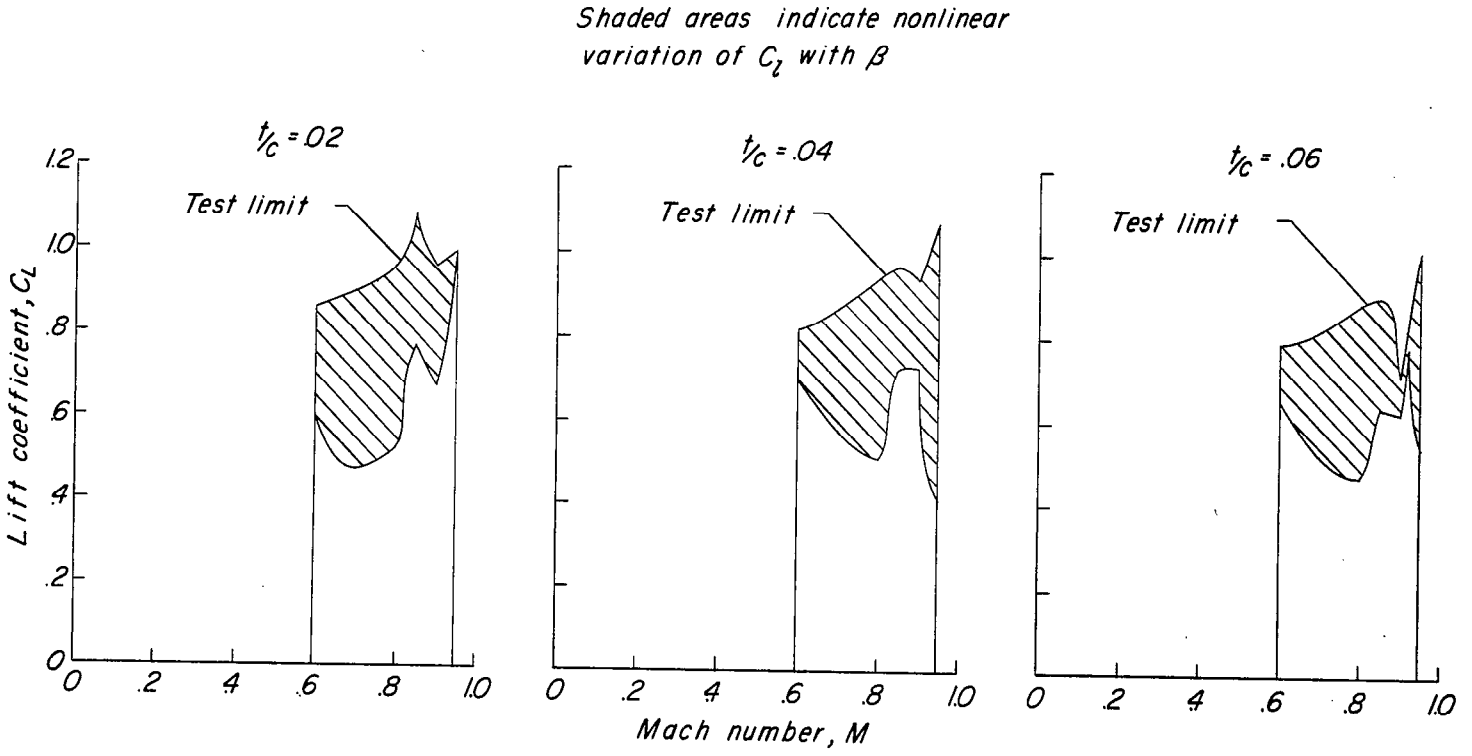

Figure 20.- Summary figure showing test limits and areas in which the variation of C_l with β was generally nonlinear.